

Generalized $\mathbb{Z}_2 \times \mathbb{Z}_2$ in Scaling neutrino Majorana mass matrix and baryogenesis via flavored leptogenesis

Roopam Sinha^{*}, Rome Samanta [†], Ambar Ghosal[‡]

Saha Institute of Nuclear Physics, HBNI, 1/AF Bidhannagar, Kolkata 700064, India

July 30, 2018

Abstract

We investigate the consequences of a generalized $\mathbb{Z}_2 \times \mathbb{Z}_2$ symmetry on a scaling neutrino Majorana mass matrix. It enables us to determine definite analytical relations between the mixing angles θ_{12} and θ_{13} , maximal CP violation for the Dirac type and vanishing for the Majorana type. Beside the other testable predictions on the low energy neutrino parameters such as $\beta\beta_{0\nu}$ decay matrix element $|M_{ee}|$ and the light neutrino masses $m_{1,2,3}$, the model also has intriguing consequences from the perspective of leptogenesis. With the assumption that the required CP violation for leptogenesis is created by the decay of lightest (N_1) of the heavy Majorana neutrinos, only τ -flavored leptogenesis scenario is found to be allowed in this model. For a normal (inverted) ordering of light neutrino masses, θ_{23} is found to be less (greater) than its maximal value, for the final baryon asymmetry Y_B to be in the observed range. Besides, an upper and a lower bound on the mass of N_1 have also been estimated. Effect of the heavier neutrinos $N_{2,3}$ on final Y_B has been worked out subsequently. The predictions of this model will be tested in the experiments such as nEXO, LEGEND, GERDA-II, T2K, NO ν A, DUNE etc.

^{*}roopam.sinha@saha.ac.in

[†]rome.samanta@saha.ac.in

[‡]ambar.ghosal@saha.ac.in

1 Introduction

The neutrino oscillation data, adhering to the bound on the sum of the three electroweak neutrino masses and the results of $\beta\beta_{0\nu}$ decay experiments severely constrain the textures of light neutrino mass matrix. Admissible textures of the mass matrix satisfying the above experimental constraints thus can be tested in future through their predictions regarding the yet unresolved issues such as the hierarchy of neutrino masses, octant determination of θ_{23} , and particularly, CP violation in the leptonic sector which might have implication on the matter-antimatter asymmetry of the universe. Besides, if neutrino is a Majorana particle, the prediction of Majorana phases will also serve as an added ingredient to discriminate different models. From the symmetry point of view thus it is a challenging task to integrate theoretical considerations involving different symmetry/ansatz in addition to the Standard Model (SM).

Recently, the idea of residual symmetry [1, 2] has attracted much attention to explore the flavor structure of light neutrino mass matrix. In this approach, the neutrino mass matrix is attributed some residual or remnant symmetry of a horizontal flavor group. It can be shown that the Majorana type nondegenerate light neutrinos lead to an invariance of the effective light neutrino mass matrix under a $\mathbb{Z}_2 \times \mathbb{Z}_2$ symmetry accompanied with a charged lepton mass matrix that enjoys a \mathbb{Z}_n invariance with $n > 2$ [1]. Now it is a challenging task to find out larger symmetry groups which embed these remnant symmetries. Nevertheless, for some predictive residual symmetries, a list of horizontal symmetry groups has been addressed by Lam [1]. In addition, viability of Coxeter groups as horizontal symmetries in the leptonic sector has been studied recently in Ref. [3]. Although some of the groups that belong to the Coxeter class have been analyzed in literature (e.g., S_4), still there are scopes for a detail study of these groups in the leptonic sector, specifically in the context of grand unified model such as SO(10) that contains Coxeter group as a built-in symmetry [4]. Furthermore, to constrain the CP violating phases, a $\mu\tau$ -interchange symmetry has been used to implement a nonstandard CP transformation in Ref. [5]. Inspired by these well accepted road maps that redirect physicists towards the quest for an ultimate elusive model, in the present work we study the effect of a generalized $\mathbb{Z}_2 \times \mathbb{Z}_2$ [6] that replicates scaling ansatz [7, 8] in conjunction with a nonstandard CP transformation on light neutrino Majorana mass matrix.

We first consider a general neutrino mass matrix M_ν^0 with scaling ansatz invariance as an effective low energy symmetry and following residual symmetry approach, interpret the latter as a residual $\mathbb{Z}_2 \times \mathbb{Z}_2$ symmetry. Due to the outcome of a vanishing reactor angle θ_{13} (which is excluded by experiment at more than 5.2σ [9]), we further use these \mathbb{Z}_2 generators to implement CP transformations. Thus instead of an ordinary $\mathbb{Z}_2 \times \mathbb{Z}_2$ symmetry, we now demand a generalized $\mathbb{Z}_2 \times \mathbb{Z}_2$ as an effective residual symmetry that extend the scaling ansatz to its complex counterpart. In this case, having a more complicated scaling relationship between its elements, the resultant mass matrices (depending upon the ways of implementation of the sym-

metry, actually there are two light neutrino mass matrices) are further reconstructed through the type-I seesaw mechanism which incorporates three right chiral singlet neutrino fields N_{iR} ($i = 1, 2, 3$) in addition to the regular SM field contents. Although it is nontrivial to combine a flavor and a CP symmetry [10–12], a consistent definition for both of them is possible when they satisfy certain condition—usually known as the consistency condition [11–13]. However, at low energy this combined symmetry should be broken to different symmetries in the neutrino and the charged lepton sector, since it is known that at least a common residual CP symmetry in both the sector would imply a vanishing CP violation [10, 11, 13]. Although here we do not focus on the explicit construction of the high energy flavor group, throughout the analysis we assume a diagonal and nondegenerate charged lepton mass matrix which is protected by a residual symmetry G_ℓ after the spontaneous breaking of the combination of CP and flavor symmetry at high energy [10, 13, 14]. Depending upon the breaking pattern, there may also be a trivial or a nontrivial CP symmetry in the charged lepton sector [15]. However, as pointed out, the final residual CP symmetries in both the sectors should be different. One can also construct a minimal high energy group from a bottom-up approach knowing the symmetry in the neutrino sector and then finding the symmetry in the charged lepton sector with the automorphism condition as described in Ref [16, 17].

Finally, using the oscillation constraints, tantalizing predictions on the low energy parameters such as neutrino masses, neutrinoless double beta decay, CP violating phases are obtained. Due to the presence of three massive right handed (RH) neutrinos, baryogenesis via leptogenesis scenario is also explored. Interesting conclusions such as octant sensitivity of the atmospheric mixing angle θ_{23} , preconditioned by the observed range of the final baryon asymmetry Y_B and nonoccurrence of unflavored leptogenesis are also drawn.

The paper is organized as follows. Section 2 contains a brief discussion on residual symmetry and scaling ansatz with a possible modification to the ansatz by extending the former with a nonstandard CP transformation. In section 3 we discuss a type-I seesaw extension of the analysis made in the previous section. Section 4 contains a discussion about baryogenesis via leptogenesis scenario related to the present model. In section 5 we present detail results of the numerical analysis. A discussion on the sensitivity of the heavier neutrinos to the obtained results for the final Y_B is presented in section 6. Section 7 concludes the entire discussion with some promising remarks.

2 Modification to scaling neutrino mass matrix with generalized $\mathbb{Z}_2 \times \mathbb{Z}_2$

Before going to an explicit details of our work, let us first discuss the residual $\mathbb{Z}_2 \times \mathbb{Z}_2$ symmetry proposed in Ref. [1]. A Majorana neutrino mass matrix M_ν enjoys a $\mathbb{Z}_2 \times \mathbb{Z}_2$ flavor symme-

try which can be envisaged as a remnant symmetry of some horizontal flavor group. These horizontal symmetry groups are preferably finite groups since in that case the theory has a more predictive power due to the discrete number of choices for the residual symmetries G_i [1]. A bottom up as well as a top down approach for a viable horizontal group has been studied in the first one of Ref. [1]. There are plenty of horizontal groups that have been explored in the literature, among them finite groups such as O_h [18], \mathbb{Z}_m [19], $\mathbb{Z}_m \times \mathbb{Z}_n$ [20], D_n [21], S_4 [22], A_4 [23], $\Delta(27)$ [24] and infinite groups such as $SO(3)$ and $SU(3)$ [25] have drawn much attention.

A linear transformation of the neutrino fields $\nu_{L\alpha} \rightarrow G_{\alpha\beta}\nu_{L\beta}$ leads to an invariance of an effective neutrino Majorana mass term

$$-\mathcal{L}_{mass}^\nu = \frac{1}{2}\bar{\nu}_{L\alpha}^C (M_\nu)_{\alpha\beta}\nu_{L\beta} + \text{h.c.}, \quad (2.1)$$

if the mass matrix M_ν satisfies the invariance equation

$$G^T M_\nu G = M_\nu. \quad (2.2)$$

Here G is a 3×3 unitary matrix in flavor basis. It has been shown in Ref. [1] that if an unitary matrix U diagonalizes M_ν then the matrix $U' = GU$ also does so where U' satisfies the condition

$$GU = Ud \quad \text{with} \quad d_{lm} = \pm\delta_{lm}. \quad (2.3)$$

Among the eight possible choices for d , only two of them can be shown to be independent on account of the relation $d_a d_b = d_b d_a = d_c$, which implies $G_a G_b = G_b G_a = G_c$ with $a \neq b \neq c$. These two independent G matrices define a $\mathbb{Z}_2 \times \mathbb{Z}_2$ symmetry since $d^2 = G^2 = I$ as dictated by Eq.(2.3). Thus given a mass matrix M_ν , one can obtain U consistent with the symmetries of M_ν . From which G_a 's can be obtained as

$$G_a = U d_a U^\dagger \quad (2.4)$$

with $a = 1, 2, 3$. Since $G^2 = I$ implies $\det G = \pm 1$, one can choose the independent d matrices corresponding to any value for the determinant of the G matrices. Here without loss of generality, we choose to proceed with $\det G = +1$ that corresponds to the structure of d matrices as $d_1 = \text{diag}(1, -1, -1)$, $d_2 = \text{diag}(-1, 1, -1)$ and $d_3 = d_1 d_2$.

Basically for an arbitrary mixing matrix U , one can construct a unique G , however the reverse is not true due to the degeneracies in the eigenvalues of d_a matrices. From this point, the implementation of the residual symmetry to the neutrino mass matrix takes different paths. Given a leading order mixing matrix, e.g. $U^{\mu\tau}$, construction of G matrices are unique, then for a particular G matrix, one might or might not have $U^{\mu\tau}$. Papers such as [2] discuss scenarios like soft breaking of one of the two residual symmetries such that presence of the other with its degenerate eigenvalues enhances the degrees of choice of the mixing matrix in accordance with the phenomenological requirement. On the other hand, in Ref. [5, 6, 26], as a more

predictive scenario, invariance of the neutrino mass matrix under an extended $\mu\tau$ symmetry ($\text{CP}^{\mu\tau}$ or CP transformation with the $\mu\tau$ -symmetry) has been considered. Both the schemes have their own uniqueness in terms of the predictions on the low energy neutrino parameters. However, in this work, we follow the second approach due to its robust predictions on CP violating phases which are related to the matter antimatter asymmetry of the universe [27].

We interpret the Strong Scaling Ansatz (SSA) proposed in Ref. [7], as a residual $\mathbb{Z}_2 \times \mathbb{Z}_2$ symmetry. Since SSA leads to a vanishing θ_{13} , a possible modification to this has been made by generalizing the two independent ordinary \mathbb{Z}_2 invariance to their complex counterpart, i.e., two independent \mathbb{Z}_2^{CP} invariance. Thus the SSA has been extended to its complex version by means of a generalized $\mathbb{Z}_2 \times \mathbb{Z}_2$ symmetry (see Ref. [6] for another such extension in case of TBM mixing). Let's discuss now the exact methodology of our analysis:

We consider a column wise scaling relations in the elements of M_ν^0 in flavor space as

$$\frac{(M_\nu^0)_{e\mu}}{(-M_\nu^0)_{e\tau}} = \frac{(M_\nu^0)_{\mu\mu}}{(-M_\nu^0)_{\mu\tau}} = \frac{(M_\nu^0)_{\tau\mu}}{(-M_\nu^0)_{\tau\tau}} = k, \quad (2.5)$$

where k is a real and positive dimensionless scaling factor. The superscript '0' on M_ν symbolizes SSA as a leading order matrix in this analysis. Now the structure for M_ν^0 dictated by the ansatz of Eq.(2.5) comes out as

$$M_\nu^0 = \begin{pmatrix} P & -Qk & Q \\ -Qk & Rk^2 & -Rk \\ Q & -Rk & R \end{pmatrix}. \quad (2.6)$$

Here P, Q, R are a priori unknown, complex mass dimensional quantities. The minus sign in Eq.(2.5) has been considered to be in conformity with the PDG convention [28]. The matrix in Eq.(2.6) is diagonalized by a unitary matrix U^0 having a form

$$U^0 = \begin{pmatrix} c_{12}^0 & s_{12}^0 e^{i\alpha} & 0 \\ -\frac{ks_{12}^0}{\sqrt{1+k^2}} & \frac{kc_{12}^0}{\sqrt{1+k^2}} e^{i\alpha/2} & \frac{1}{\sqrt{1+k^2}} e^{i\beta/2} \\ \frac{s_{12}^0}{\sqrt{1+k^2}} & -\frac{c_{12}^0}{\sqrt{1+k^2}} e^{i\alpha/2} & \frac{k}{\sqrt{1+k^2}} e^{i\beta/2} \end{pmatrix}, \quad (2.7)$$

where $c_{12}^0 = \cos \theta_{12}^0$, $s_{12}^0 = \sin \theta_{12}^0$ which are calculated in terms of the parameters of M_ν^0 , and α, β represents the Majorana phases. SSA predicts a vanishing θ_{13} (hence no measurable leptonic Dirac CP-violation) as one can see from Eq.(2.7) and an inverted neutrino mass ordering (i.e., $m_{2,1} > m_3$), with $m_3 = 0$. As previously mentioned, one needs to modify the ansatz to generate a non-zero θ_{13} . Now using the paradigm of residual symmetry as described in the earlier part of this section, one can calculate the G_a matrices using the relation

$$G_a^{(k)} = U^0 d_a U^{0\dagger} \quad (2.8)$$

with $G_a^{(k)}$ as the \mathbb{Z}_2 generators for a scaling ansatz invariant M_ν . Similar to Eq.(2.2), M_ν^0 will then satisfy the invariance equation

$$\left(G_a^{(k)}\right)^T M_\nu^0 G_a^{(k)} = M_\nu^0. \quad (2.9)$$

Now using Eq.(2.8) we calculate the corresponding $G_a^{(k)}$ ($a = 1, 2, 3$) matrices and present them as

$$G_1^{(k)} = \begin{pmatrix} \cos 2\theta_{12}^0 & -k(1+k^2)^{-1/2} \sin 2\theta_{12}^0 & -(1+k^2)^{-1/2} \sin 2\theta_{12}^0 \\ -k(1+k^2)^{-1/2} \sin 2\theta_{12}^0 & -(1+k^2)^{-1}(k^2 \cos 2\theta_{12}^0 + 1) & -k(1+k^2)^{-1}(1 - \cos 2\theta_{12}^0) \\ -(1+k^2)^{-1/2} \sin 2\theta_{12}^0 & -k(1+k^2)^{-1}(1 - \cos 2\theta_{12}^0) & -(1+k^2)^{-1}(k^2 + \cos 2\theta_{12}^0) \end{pmatrix}, \quad (2.10)$$

$$G_2^{(k)} = \begin{pmatrix} -\cos 2\theta_{12}^0 & k(1+k^2)^{-1/2} \sin 2\theta_{12}^0 & -(1+k^2)^{-1/2} \sin 2\theta_{12}^0 \\ k(1+k^2)^{-1/2} \sin 2\theta_{12}^0 & (1+k^2)^{-1}(k^2 \cos 2\theta_{12}^0 - 1) & -k(1+k^2)^{-1}(1 + \cos 2\theta_{12}^0) \\ -(1+k^2)^{-1/2} \sin 2\theta_{12}^0 & -k(1+k^2)^{-1}(1 + \cos 2\theta_{12}^0) & -(1+k^2)^{-1}(k^2 - \cos 2\theta_{12}^0) \end{pmatrix}, \quad (2.11)$$

$$G_3^{(k)} = \begin{pmatrix} -1 & 0 & 0 \\ 0 & (1-k^2)(1+k^2)^{-1} & 2k(1+k^2)^{-1} \\ 0 & 2k(1+k^2)^{-1} & -(1-k^2)(1+k^2)^{-1} \end{pmatrix}. \quad (2.12)$$

Note that all the $G_a^{(k)}$ matrices are symmetric by construction. Now to modify SSA, we generalize this $\mathbb{Z}_2 \times \mathbb{Z}_2$ by implementing CP transformations on the neutrino fields [29] with the \mathbb{Z}_2 generators ($G_a^{(k)} = G_a^{(k)T}$) as¹

$$\nu_{L\alpha} \rightarrow i(G_a^{(k)})_{\alpha\beta} \gamma^0 \nu_{L\beta}^C. \quad (2.13)$$

This extends the real horizontal invariance of M_ν^0 in Eq.(2.9) to its complex counterpart, i.e.

$$\left(G_a^{(k)}\right)^T M_\nu G_a^{(k)} = M_\nu^*. \quad (2.14)$$

Therefore the SSA, elucidated as a $\mathbb{Z}_2 \times \mathbb{Z}_2$ symmetry, has now been modified to an extended SSA, interpreted as a complex $\mathbb{Z}_2 \times \mathbb{Z}_2$ symmetry which is some time also referred as a generalized $\mathbb{Z}_2 \times \mathbb{Z}_2$ symmetry of M_ν [6]. In the next subsections we show that there are only two ways in which such a complex extension can be done.

2.1 Case I: Complex extension of $G_{2,3}^{(k)}$ Invariance

The complex invariance relations of M_ν related to $G_{2,3}^{(k)}$ is now written as

$$\left(G_{2,3}^{(k)}\right)^T M_\nu G_{2,3}^{(k)} = M_\nu^*, \quad (2.15)$$

¹The matrices that represent the CP symmetry should be symmetric [10].

which in turn implies

$$\left(G_1^{(k)}\right)^T M_\nu G_1^{(k)} = M_\nu \quad (2.16)$$

owing to the closure property of the $G_a^{(k)}$ ($a = 1, 2, 3$) matrices.

Eq.(2.15) leads to a most general Majorana neutrino mass matrix of the form

$$M_\nu^{MS1} = \begin{pmatrix} p & -q_1 k + i \frac{q_2}{k} & q_1 + i q_2 \\ -q_1 k + i \frac{q_2}{k} & r - \frac{s(k^2-1)}{k} + i \frac{2q_2 \kappa_+}{\sqrt{1+k^2}} & s + i \frac{q_2 \kappa_+ (k^2-1)}{k \sqrt{1+k^2}} \\ q_1 + i q_2 & s + i \frac{q_2 \kappa_+ (k^2-1)}{k \sqrt{1+k^2}} & r - i \frac{2q_2 \kappa_+}{\sqrt{1+k^2}} \end{pmatrix} \quad (2.17)$$

with

$$r = (sk + p) - q_1 \sqrt{1+k^2} \left(\kappa_+ - \frac{1}{\kappa_+} \right), \quad (2.18)$$

$$\kappa_+ = (\cot 2\theta_{12}^0 + \operatorname{cosec} 2\theta_{12}^0). \quad (2.19)$$

Here $p, q_{1,2}, r$ and s are real, mass dimensional quantities and the superscript ‘ MS ’ stands for ‘Modified Scaling’. It has already been shown in Ref. [30] that $(G_3^{(k)})^T M_\nu G_3^{(k)} = M_\nu^*$ leads to the results

$$\tan \theta_{23} = k^{-1}, \quad (2.20)$$

$$\sin \alpha = \sin \beta = \cos \delta = 0. \quad (2.21)$$

Now in the present case, the overall real $G_1^{(k)}$ (cf. Eq.(2.16)) invariance of M_ν fixes the first column of U_{PMNS} to the first column of U^0 . Therefore, one gets the relation between the solar and the reactor mixing angle as

$$|\cos \theta_{12} \cos \theta_{13}| = \cos \theta_{12}^0 \Rightarrow \sin^2 \theta_{12} = 1 - \cos^2 \theta_{12}^0 (1 + \tan^2 \theta_{13}). \quad (2.22)$$

2.2 Case II: Complex extension of $G_{1,3}^{(k)}$ Invariance

In this case, the complex invariance relations of M_ν due to $G_{1,3}^{(k)}$ can be written as

$$\left(G_{1,3}^{(k)}\right)^T M_\nu G_{1,3}^{(k)} = M_\nu^*, \quad (2.23)$$

which leads to

$$\left(G_2^{(k)}\right)^T M_\nu G_2^{(k)} = M_\nu. \quad (2.24)$$

Eq.(2.23) leads to the mass matrix M_ν^{MS2} having a form same as M_ν^{MS1} as given in Eq.(2.17) where κ_+ is replaced with $\kappa_- = -1/\kappa_+$. Similar to the previous case, a complex invariance due to $G_3^{(k)}$ leads to the predictions

$$\tan \theta_{23} = k^{-1}, \quad (2.25)$$

$$\sin \alpha = \sin \beta = \cos \delta = 0. \quad (2.26)$$

Now the overall real $G_2^{(k)}$ (cf. Eq.(2.24)) invariance of M_ν fixes the second column of U_{PMNS} to the second column of U^0 which gives rise to a relation between the solar and the reactor mixing angle as

$$|\sin \theta_{12} \cos \theta_{13}| = \sin \theta_{12}^0 \Rightarrow \sin^2 \theta_{12} = \sin^2 \theta_{12}^0 (1 + \tan^2 \theta_{13}). \quad (2.27)$$

Similar to the previous cases, complex invariance due to $G_{1,2}^{(k)}$ leads to an overall real invariance due to $G_3^{(k)}$ which leads to a vanishing θ_{13} . Thus this is a case of least interest. For both the viable cases, we determine three CP phases ($\cos \delta = 0, \alpha, \beta = 0$ or π). Thus there are 6 real free parameters $p, q_{1,2}, s, k$ and κ_+ (or θ_{12}^0) (cf. Eq.(2.17)) in both the mass matrices. However, one can trivially track the parameters k and θ_{12}^0 on account of the relations in (2.20) or (2.25) and (2.22) or (2.27). Thus the other four parameters account for one mixing angle and three neutrino masses. However, to fix the absolute neutrino mass scale, we additionally use some constraints from baryogenesis as discussed in the numerical section.

We note that the prediction of the CP phases in the extended SSA scheme are identical to the case of $\text{CP}^{\mu\tau}$ [5]. Therefore the question arises how one might distinguish the $\text{CP}^{\mu\tau}$ and the extended SSA experimentally? First of all, both the Strong Scaling Ansatz (SSA) and the $\mu\tau$ symmetry lead to $\theta_{13} = 0$ at the leading order and therefore, has to be abandoned. However, one can in principle differentiate SSA from the $\mu\tau$ reflection symmetry via their predictions of atmospheric mixing angle θ_{23} . The former in general predicts a nonmaximal θ_{23} (for $k \neq 1$) given by $\theta_{23} = \tan^{-1}(k^{-1})$ while a maximal value ($\theta_{23} = \pi/4$) is predicted by the latter.

Furthermore, in the extended scheme, besides the similar predictions for the CP phases an arbitrary nonvanishing value of the reactor mixing angle θ_{13} is predicted in both the cases (extended SSA and $\text{CP}^{\mu\tau}$). However, the prediction on the θ_{23} is different for each case. Interestingly, even after the extension, the value of θ_{23} survives for both the cases i.e., $\theta_{23} = \tan^{-1}(k^{-1})$ for the SSA as well as extended SSA and $\theta_{23} = \pi/4$ for $\mu\tau$ symmetry and its extended version ($\text{CP}^{\mu\tau}$). If experiments find a nonmaximal θ_{23} at a significant confidence level (recently there is a hint from $\text{NO}\nu\text{A}$ regarding the nonmaximality of θ_{23} at 2.6σ CL [31]) then the $\text{CP}^{\mu\tau}$ symmetry will be ruled out while our proposal of an extended SSA (that predicts a nonmaximal θ_{23} in general) will continue to survive.

Before proceeding further we should comment on the fulfillment of the consistency conditions [11–13] as mentioned in the introduction. Here we have discussed two cases. In the first one $G_{2,3}^{(k)}$ are the CP symmetries which further result in a $G_1^{(k)}$ invariance of the mass term while in the second case, the CP generators $G_{1,3}^{(k)}$ lead to an invariance of the mass term due to the $G_2^{(k)}$. Now the consistency condition in case of a \mathbb{Z}_2 group implies [13]

$$X_r \rho_r^*(g) X_r^{-1} = \rho_r(g), \quad (2.28)$$

where X_r is a unitary matrix representing CP symmetry which acts on a generic multiplet φ as

$$X_r \varphi(x) \xrightarrow{\text{CP}} X_r \varphi(x') \quad (2.29)$$

with $x' = (t, -\mathbf{x})$ and $\rho_r(g)$ is a representation for the element g of the flavor group in an irreducible representation \mathbf{r} . In our analysis, $G_i^{(k)}$'s are real, and hence, the condition in Eq.(2.28) turns out to be

$$\begin{aligned} G_{2,3}^{(k)} G_1^{(k)} (G_{2,3}^{(k)})^{-1} &= G_1^{(k)} \quad \text{for Case I;} \\ G_{1,3}^{(k)} G_2^{(k)} (G_{1,3}^{(k)})^{-1} &= G_2^{(k)} \quad \text{for Case II.} \end{aligned} \quad (2.30)$$

Since $(G_i^{(k)})^2 = 1$, $(G_i^{(k)})^{-1} = G_i^{(k)}$ and each $G_i^{(k)}$ commutes with each other, the consistency condition is trivially satisfied for both the cases. However the main challenge is to ensure that such conditions are fulfilled for the larger (embedding) symmetries [10–12] which we do not explore here in this work.

Resolving the shortcomings of SSA, both the viable modified SSA matrices, referred as M_ν^{MS1} and M_ν^{MS2} , possess intriguing phenomenology. This has been discussed in section 5 on numerical analysis. For the time being let's focus on the implementation of the symmetry in a more specific way. So far we have discussed a possible complex extension for a general M_ν , not so about the origin of the neutrino masses. This would be interesting to see the effects of generalized $\mathbb{Z}_2 \times \mathbb{Z}_2$ on a particular mechanism that generates the light neutrino masses. Obviously, the choice depends upon the phenomenological interest. Here we choose the type-I seesaw mechanism and investigate possible consequences of the generalized $\mathbb{Z}_2 \times \mathbb{Z}_2$ to explore the phenomena of baryogenesis via leptogenesis. A detailed discussion about these has been presented in the next two sections. First, we show the reconstruction of the effective modified SSA matrices through type-I seesaw mechanism with proper implementation of the symmetry on the constituent matrices (m_D and M_R). Then we discuss some aspects of baryogenesis via leptogenesis related to this scheme.

3 Reconstruction of modified scaling matrices with type-I seesaw

For the realization of generalized $\mathbb{Z}_2 \times \mathbb{Z}_2$ in the context of type-I seesaw mechanism, we define two separate 'G' matrices G_L and G_R for ν_L and N_R fields respectively. Now the CP transformations are defined on these fields as [32]

$$\nu_{L\alpha} \rightarrow i(G_L)_{\alpha\beta} \gamma^0 \nu_{L\beta}^C, \quad N_{R\alpha} \rightarrow i(G_R)_{\alpha\beta} \gamma^0 N_{R\beta}^C. \quad (3.1)$$

With m_D as a Dirac type and M_R as a diagonal nondegenerate Majorana type mass matrix, the Lagrangian for type-I seesaw

$$-\mathcal{L} = \bar{N}_{iR}(m_D)_{i\alpha}l_{L\alpha} + \frac{1}{2}\bar{N}_{iR}(M_R)_i\delta_{ij}N_{jR}^C + \text{h.c.} \quad (3.2)$$

leads to the effective 3×3 light neutrino Majorana mass matrix M_ν as

$$M_\nu = -m_D^T M_R^{-1} m_D. \quad (3.3)$$

Now the invariance of the mass terms of Eq.(3.2) under the CP transformations defined in Eq.(3.1) leads to the relations

$$G_R^\dagger m_D G_L = m_D^*, \quad G_R^\dagger M_R G_R^* = M_R^*. \quad (3.4)$$

Eqs.(3.3) and (3.4) together imply $G_L^T M_\nu G_L = M_\nu^*$. Now, specifying G_L by $G_i^{(k)}$, we obtain the key equation

$$\left(G_i^{(k)}\right)^T M_\nu G_i^{(k)} = M_\nu^*. \quad (3.5)$$

Since M_R is taken to be diagonal i.e., $M_R = \text{diag}(M_1, M_2, M_3)$, the corresponding symmetry generator matrix G_R is diagonal [32] with entries ± 1 , i.e.,

$$(G_R)_{lm} = \pm \delta_{lm}. \quad (3.6)$$

which implies for each G_L , there are eight different structures for G_R that correspond to eight different choices of m_D . However, a straightforward computation shows that for the case-I, the G_R matrix compatible with $G_2^{(k)}$ and $G_3^{(k)}$ should be taken as $(G_R)_2 = \text{diag}(1, 1, 1)$ and $(G_R)_3 = \text{diag}(-1, -1, -1)$ respectively. Similarly for Case-II also, those are taken as $(G_R)_1 = \text{diag}(1, 1, 1)$ and $(G_R)_3 = \text{diag}(-1, -1, -1)$ for $G_1^{(k)}$ and $G_3^{(k)}$. It can be shown that all the other choices of G_R are incompatible with scaling symmetry. Therefore, the first of Eq.(3.4) leads to

$$\begin{aligned} m_D G_3 &= -m_D^*, m_D G_2 = m_D^* && \text{for Case-I} \\ m_D G_3 &= -m_D^*, m_D G_1 = m_D^* && \text{for Case-II.} \end{aligned} \quad (3.7)$$

For both the cases as discussed above, the most general form of m_D that satisfies the constraints of Eq.(3.7) can be parameterized as

$$m_D^{MS} = \begin{pmatrix} a & b_1 + ib_2 & -b_1/k + ib_2k \\ e & c_1 + ic_2 & -c_1/k + ic_2k \\ f & d_1 + id_2 & -d_1/k + id_2k \end{pmatrix} \quad (3.8)$$

with

$$b_1 = \pm ak(1 + k^2)^{-1/2} \kappa_\pm, \quad (3.9)$$

$$c_1 = \pm ek(1+k^2)^{-1/2}\kappa_{\pm}, \quad (3.10)$$

$$d_1 = \pm fk(1+k^2)^{-1/2}\kappa_{\pm}. \quad (3.11)$$

Here the ‘ \pm ’ sign in the expressions of b_1, c_1 and d_1 are for Case-I and Case-II respectively. In Eq.(3.8) a, e, f, b_2, c_2 and d_2 are six a priori unknown real mass dimensional quantities and k is a real, positive, dimensionless parameter. Now using the seesaw relation in Eq.(3.3), it is easy to reconstruct the effective mass matrices M_{ν}^{MS1} and M_{ν}^{MS2} for Case-I and Case-II respectively. In Table 1, we present the parameters of the effective light neutrino mass matrix in terms of the Dirac and Majorana components.

Table 1: Parameters of M_{ν} .

$p = -\left(\frac{a^2}{M_1} + \frac{e^2}{M_2} + \frac{f^2}{M_3}\right)$ $q_1 = -\frac{\kappa_{\pm} p}{\sqrt{1+k^2}}$ $q_2 = -k\left(\frac{ab_2}{M_1} + \frac{ec_2}{M_2} + \frac{fd_2}{M_3}\right)$ $s = -\frac{\kappa_{\pm}^2 pk}{1+k^2} + k\left(\frac{b_2^2}{M_1} + \frac{c_2^2}{M_2} + \frac{d_2^2}{M_3}\right)$ $r = (sk + p) - q_1\sqrt{1+k^2}\left(\kappa_{\pm} - \frac{1}{\kappa_{\pm}}\right)$
--

Once again ‘ \pm ’ sign in κ are for Case-I and Case-II respectively.

Before concluding this section we would like to address the following: It clear from Eq.(2.12) and Eq.(3.6)) that the matrices G_L and G_R are of different form. This is since we choose to work in a basis where M_R is diagonal but m_D is not (“leptogenesis basis” [32]). However that does not mean that the left handed and right handed field must transform differently. The form of G_R , i.e., $G_R = \text{diag}(\pm 1, \pm 1, \pm 1)$ is obtained purely for the diagonal M_R matrix. In principle one may assume same residual symmetry (say G) in the matrices m_D and M_R when both of them are nondiagonal. However, in a basis where M_R is diagonal the symmetry in the nondiagonal M_R ultimately changes to $G_R = \text{diag}(\pm 1, \pm 1, \pm 1)$ while the symmetry in the left handed field remains the same.

To see this explicitly, we consider the Lagrangian of Eq.(3.2) with a nondiagonal M_R . Now M_R could be diagonalized by a unitary matrix U_N as

$$U_N^\dagger M_R U_N = M_R^d = \text{diag}(M_1, M_2, M_3), \quad (3.12)$$

where M_R^d is a real diagonal matrix with nondegenerate eigenvalues. Eq.(3.4) can now be rewritten as

$$G^\dagger m_D G = m_D^*, \quad G^\dagger M_R G^* = M_R^*, \quad (3.13)$$

where we have assumed same symmetry for both the fields. Now the second equation of Eq.(3.13) and Eq.(3.12) together imply

$$U_N^T G^\dagger U_N = d^\dagger, \quad (3.14)$$

where d is a diagonal matrix with $d_{jj} = \pm 1$. In the basis where the RH neutrino mass matrix is diagonal one can have a modified Dirac matrix as

$$m_D \rightarrow m'_D = U_N^\dagger m_D. \quad (3.15)$$

Thus the first equation of Eq.(3.13) and Eq.(3.14) give

$$U_N^* d^\dagger U_N^\dagger m_D G = m_D^* \quad \text{or} \quad d^\dagger m'_D G = m_D^*, \quad (3.16)$$

where m'_D is defined in Eq.(3.15). Thus starting from a basis where M_R is nondiagonal, we obtain the identical complex symmetry condition on the Dirac mass matrix as given in Eq.(3.4) in the basis where M_R is diagonal. This is worth mentioning that the matrix d is basically the matrix G_R of Eq.(3.6) since they both are diagonal with entries ± 1 .

4 Baryogenesis via leptogenesis

Baryogenesis via leptogenesis [33, 34] is a phenomena where CP violating and out of equilibrium decays from heavy Majorana neutrinos generate a lepton asymmetry which is thereafter converted into baryon asymmetry by sphaleron transition [35]. The pertinent Lagrangian for the process can be written as

$$-\mathcal{L} = \lambda_{i\alpha} \bar{N}_{Ri} \tilde{\phi}^\dagger l_{L\alpha} + \frac{1}{2} \bar{N}_{iR} (M_R)_i \delta_{ij} N_{jR}^C + \text{h.c.} \quad (4.1)$$

where $l_{L\alpha} = (\nu_{L\alpha} \ e_{L\alpha})^T$ is the SM lepton doublet of flavor α , and $\tilde{\phi} = i\tau_2 \phi^*$ with $\phi = (\phi^+ \ \phi^0)^T$ being the Higgs doublet. Thus the possible decays of N_i from Eq.(4.1) are $N_i \rightarrow e_\alpha^- \phi^+$, $N_i \rightarrow \nu_\alpha \phi^0$, $N_i \rightarrow e_\alpha^+ \phi^-$, and $N_i \rightarrow \nu_\alpha^C \phi^{0*}$. The CP asymmetry parameter ε_i^α that accounts for the required CP violation, arises due to the interference between the tree level, one loop self energy, one loop vertex N_i -decay diagrams [33] and has a general expression [36]

$$\varepsilon_i^\alpha = \frac{1}{4\pi v^2 h_{ii}} \sum_{j \neq i} \left\{ \text{Im}[h_{ij}(m_D)_{i\alpha}(m_D^*)_{j\alpha}] g(x_{ij}) + \frac{\text{Im}[h_{ji}(m_D)_{i\alpha}(m_D^*)_{j\alpha}]}{1 - x_{ij}} \right\} \quad (4.2)$$

where $h \equiv m_D m_D^\dagger$, $\langle \phi^0 \rangle = v/\sqrt{2}$ so that $m_D = v\lambda/\sqrt{2}$, and $x_{ij} = M_j^2/M_i^2$. Furthermore, the loop function $g(x_{ij})$ has the expression

$$g(x_{ij}) = \frac{\sqrt{x_{ij}}}{1 - x_{ij}} + f(x_{ij}) \quad (4.3)$$

with

$$f(x_{ij}) = \sqrt{x_{ij}} \left[1 - (1 + x_{ij}) \ln \left(\frac{1 + x_{ij}}{x_{ij}} \right) \right]. \quad (4.4)$$

Before going to the explicit calculation of ε_i^α related to this model, let's address some important issues related to leptogenesis. For a hierarchical scenario, e.g., $M_3 \gg M_2 \gg M_1$, it can be shown that only the decays of N_1 matter for the creation of lepton asymmetry while the latter created from the heavier neutrinos get washed out [37]. Obviously there are certain circumstances when the decays of $N_{2,3}$ are also significant [38]. Again, flavor plays an important role in the phenomena of leptogenesis [39]. Assuming the temperature scale of the process $T \sim M_1$, the rates of the Yukawa interaction categorize leptogenesis into three categories. 1) $T \sim M_1 > 10^{12}$ GeV, when all interactions with all flavors are out of equilibrium: unflavored leptogenesis. In this case all the flavors are indistinguishable and thus the total CP asymmetry is a sum over all flavors, i.e., $\varepsilon_i = \sum_\alpha \varepsilon_i^\alpha$. 2) 10^9 GeV $< T \sim M_1 < 10^{12}$ GeV, when only the τ flavor is in equilibrium: τ -flavored leptogenesis. In this regime there are two relevant CP asymmetry parameters; ε_i^τ and $\varepsilon_i^{(2)} = \varepsilon_i^e + \varepsilon_i^\mu$. 3) $T \sim M_1 < 10^9$ GeV, when all the flavors (e, μ, τ) are in equilibrium and distinguishable: fully flavored leptogenesis.

Note that the flavor sum on α leads to a vanishing value of the second term in Eq.(4.2), since

$$\sum_\alpha \text{Im}[h_{ji}(m_D)_{i\alpha}(m_D^*)_{j\alpha}] = \text{Im}[h_{ji}h_{ij}] = \text{Im}|h_{ji}|^2 = 0, \quad (4.5)$$

while the first term is proportional to $\text{Im}(h_{ij}^2)$. Now for both the cases in our model, h has a generic form

$$h = \begin{pmatrix} a^2(1 + \kappa_\pm^2) + b_2^2(1 + k^2) & ae(1 + \kappa_\pm^2) + (1 + k^2)b_2c_2 & af(1 + \kappa_\pm^2) + (1 + k^2)b_2d_2 \\ ae(1 + \kappa_\pm^2) + (1 + k^2)b_2c_2 & e^2(1 + \kappa_\pm^2) + c_2^2(1 + k^2) & ef(1 + \kappa_\pm^2) + (1 + k^2)c_2d_2 \\ af(1 + \kappa_\pm^2) + (1 + k^2)b_2d_2 & ef(1 + \kappa_\pm^2) + (1 + k^2)c_2d_2 & f^2(1 + \kappa_\pm^2) + d_2^2(1 + k^2) \end{pmatrix} \quad (4.6)$$

with ‘ \pm ’ sign in κ are for Case-I and Case-II respectively. Note that the matrix h in Eq.(4.6) is real. Therefore, unflavored leptogenesis which is relevant for the high temperature regime does not take place for any N_i in this model. As mentioned earlier in this section, in general any initial asymmetry produced by the heavier RH neutrinos ($N_{2,3}$) get washed out by lepton number violating N_1 related interaction [37] unless some fine tuned conditions as discussed in the Sec.6 are satisfied. Thus with the assumption that only the decay of N_1 matters in generating the CP asymmetry, ε_1 is the relevant quantity for unflavored leptogenesis, but it vanishes in this model.

Next, we concentrate on computing the α -flavored CP asymmetry in terms of x_{12} , x_{13} and the elements of m_D . These are necessary ingredients for the fully flavored and the τ -flavored

regimes. We find a vanishing value² of ε_1^e while $\varepsilon_1^{\mu,\tau}$ are calculated as

$$\varepsilon_1^\mu = \zeta[b_2k^2(\chi_1 + \chi_2) + b_1(\chi_3 + \chi_4) - b_2\chi_5] = -\varepsilon_1^\tau. \quad (4.7)$$

In Eq.(4.7) the real parameters ζ and χ_i ($i = 1 - 5$) are defined as

$$\zeta = [4\pi v^2(b_1^2 + (a^2 + b_1^2 + b_2^2)k^2 + b_2k^4)]^{-1}, \quad (4.8)$$

$$\chi_1 = b_2(1 + k^2)[c_1c_2A_{12} + d_1d_2A_{13}], \quad (4.9)$$

$$\chi_2 = c[c_1eA_{12} + d_1fA_{13}], \quad (4.10)$$

$$\chi_3 = b_2(1 + k^2)[c_1^2A_{12} - k^2(c_2^2A_{12} - d_2^2A_{13}) + d_1^2A_{13}], \quad (4.11)$$

$$\chi_4 = -ak^2[c_2eA_{12} + d_2fA_{13}], \quad (4.12)$$

$$\chi_5 = (1 + k^2)[c_1c_2A_{12} + d_1d_2A_{13}] \quad (4.13)$$

where $A_{ij} = g(x_{ij}) + (1 - x_{ij})^{-1}$.

Now for $T \sim M_1 < 10^9$ GeV regime, Y_B is well approximated with [39]

$$Y_B \simeq -\frac{12}{37g^*} \left[\varepsilon_i^e \eta \left(\frac{151}{179} \tilde{m}_e \right) + \varepsilon_i^\mu \eta \left(\frac{344}{537} \tilde{m}_\mu \right) + \varepsilon_i^\tau \eta \left(\frac{344}{537} \tilde{m}_\tau \right) \right] \quad (4.14)$$

where \tilde{m}_α are the wash-out masses, defined as

$$\tilde{m}_\alpha = \frac{|(m_D)_{1\alpha}|^2}{M_1} \quad (\alpha = e, \mu, \tau), \quad (4.15)$$

$\eta(\tilde{m}_\alpha)$ is the efficiency factor that accounts for the inverse decay and the lepton number violating scattering processes and g^* is the number of relativistic degrees of freedom in the thermal bath having a value $g^* \approx 106.75$ in the SM. And for 10^9 GeV $< T \sim M_1 < 10^{12}$ GeV, Y_B is approximated with [39]

$$Y_B \simeq -\frac{12}{37g^*} \left[\varepsilon_i^{(2)} \eta \left(\frac{417}{589} \tilde{m}_2 \right) + \varepsilon_i^\tau \eta \left(\frac{390}{589} \tilde{m}_\tau \right) \right], \quad (4.16)$$

where $\tilde{m}_2 = \sum_{\alpha=e,\mu} \tilde{m}_\alpha = \tilde{m}_e + \tilde{m}_\mu$ and $\varepsilon_i^{(2)} = \sum_{\alpha=e,\mu} \varepsilon_i^\alpha = \varepsilon_i^e + \varepsilon_i^\mu$.

At the end we would like to mention the following: Existing literature such as [32, 40, 41] also discussed the phenomena of leptogenesis under the framework of residual CP symmetry. They also pointed out the nonoccurrence of unflavored leptogenesis and only the viability of τ -flavored scenario in case of a preserved residual CP symmetry (in particular $CP^{\mu\tau}$) in the neutrino sector. Interestingly, Ref. [32, 40] pointed out M_1 to be $\mathcal{O}(10^{11}$ GeV) to produce Y_B in the observed range which is also true for our analysis (see numerical section). However the final analysis in Ref. [32, 40] is to some extent different from our analysis. In [32, 40], the authors present the variation of Y_B with a single model parameter for a fixed value of $M_1(5 \times 10^{11}$

²This is also true for $CP^{\mu\tau}$ [40, 41] since $(m_D)_{1e}$, $(m_D)_{2e}$ and h are all real as in our case.

GeV) and for the best fit values of the oscillation parameters. In our analysis, we stick to the near best fit values of the Yukawa parameters for which Y_B is positive. However, as we shall see in the numerical section, we can only constrain the Yukawa parameters scaled by the RH neutrino masses. Thus for a particular set of scaled parameters we can vary the value of M_1 freely and obtain an upper and a lower bound on M_1 corresponding to the observed upper and lower bound of Y_B . Another point is that in our analysis the sign of the final Y_B depends upon the primed Yukawa parameters and not on the CP phases. However, Ref. [41] discusses how in a residual CP scheme the sign of Y_B depends upon the low energy CP phases through a correction to the m_D matrix.

5 Numerical analysis: methodology and discussion

In order to assess the viability of our theoretical conjecture and consequent outcomes, we present a numerical analysis in substantial detail for both the viable cases. Our method of analysis and organization are as follows. First, we utilize the (3σ) values of globally fitted neutrino oscillation data (Table 2), together with an upper bound of 0.23 eV [27] on the sum of the light neutrino masses arising from PLANCK. To fix the absolute neutrino mass scale we assume $m_{max} \approx \sqrt{|\Delta m_{23}|^2}$ which is in general used in the type-I seesaw like models to be consistent with Davidson-Ibarra bound [42]. We also discard the possibility of weak washout scenario $K_\alpha = \tilde{m}_\alpha/10^{-3} < 1$ which strongly depends upon the initial conditions and likely to be disfavored by the current oscillation data [43]. We first constrain the parameter space in terms of the rescaled (primed) parameters defined below.

$$\begin{aligned}
 a &\longrightarrow a' = \frac{a}{\sqrt{M_1}}, e \longrightarrow e' = \frac{e}{\sqrt{M_2}}, \\
 f &\longrightarrow f' = \frac{f}{\sqrt{M_2}}, b_{1,2} \longrightarrow b'_{1,2} = \frac{b_{1,2}}{\sqrt{M_1}}, \\
 c_{1,2} &\longrightarrow c'_{1,2} = \frac{c_{1,2}}{\sqrt{M_2}}, d_{1,2} \longrightarrow d'_{1,2} = \frac{d_{1,2}}{\sqrt{M_3}}.
 \end{aligned} \tag{5.1}$$

Then we explore the predictions of the present model in the context of the $\beta\beta_{0\nu}$ experiments for each of the cases. Finally, in order to estimate the value of Y_B we make use of these constrained parameters with a subtlety. Since we have only constrained the primed parameters, there remains a freedom of various set of independent choices for the parameters of m_D (unprimed) along with M_i , for a given set of primed parameters. Note that for the computation of Y_B we need to feed the unprimed parameters and M_i separately. However, for the entire parameter space of primed parameters, it is impractical to generate the unprimed ones for different values of M_i as one ends up with infinite number of choices. For this, from the entire parameter space of the primed parameters, we have considered only that set of primed parameters which corresponds to a positive value of Y_B (sign of Y_B depends upon the primed parameters) and observables that lie near their best-fit values as dictated by the oscillation data. Then varying M_1 , we generate the corresponding unprimed set (parameters of m_D). Note that here we take

only M_1 as the free parameter assuming $M_{i+1}/M_i = 10^3$ for $i = 1, 2$. Thus for each value of M_1 and corresponding unprimed parameters we obtain the final baryon asymmetry Y_B . Since Y_B has an observed upper and lower bound, we get an upper and a lower bound for M_1 also. Let's now present the numerical results of our analysis in systematic way.

Constraints from oscillation data

For each of the viable cases, both the normal ordering (NO) and inverted ordering (IO) of light neutrino masses are found to be permitted over a respectable size of parameter space consistent with the aforementioned experimental constraints. This is interesting since the ordinary SSA predicts $m_3 = 0$, and thus, inverted light neutrino mass ordering (see Sec.2). However in the extended case both the mass orderings are allowed due to the fact that the matrices M_ν^{MS1} and M_ν^{MS2} have nonzero determinant. The ranges of the primed parameters for both the cases I and II are graphically shown in Fig.1-4. These plots are basically two dimensional projection of a coupled six dimensional parameter space. In order to constrain the parameter space, the explicit analytic relations that have been implemented in the computer program can be found in Ref. [44] which discusses explicit expressions for the masses and mixing angles for a general 3×3 Majorana mass matrix.

In both the cases, reduction in the number of parameters upon rescaling led to a constrained range for each of the light neutrino masses as depicted in Table 3. It has been found that all the light neutrino mass spectrum are hierarchical. Interestingly, though the upper bound on $\Sigma_i m_i$ is fed in as an input constraint, the bound has not been reached up in our model irrespective of the mass ordering. The predictions on $\Sigma_i m_i$ are tabulated in Table 3 for each of the cases.

Table 2: Input values fed into the analysis [45].

Parameters	θ_{12} (degrees)	θ_{23} (degrees)	θ_{13} (degrees)	Δm_{21}^2 $10^{-5}(\text{eV}^2)$	$ \Delta m_{31}^2 $ $10^{-3}(\text{eV}^2)$
3σ ranges/ others	31.29 – 35.91	38.3 – 53.3	7.87 – 9.11	7.02 – 8.09	2.32 – 2.59
Best fit values (NO)	33.48	42.3	8.50	7.50	2.46
Best fit values (IO)	33.48	49.5	8.51	7.50	2.45

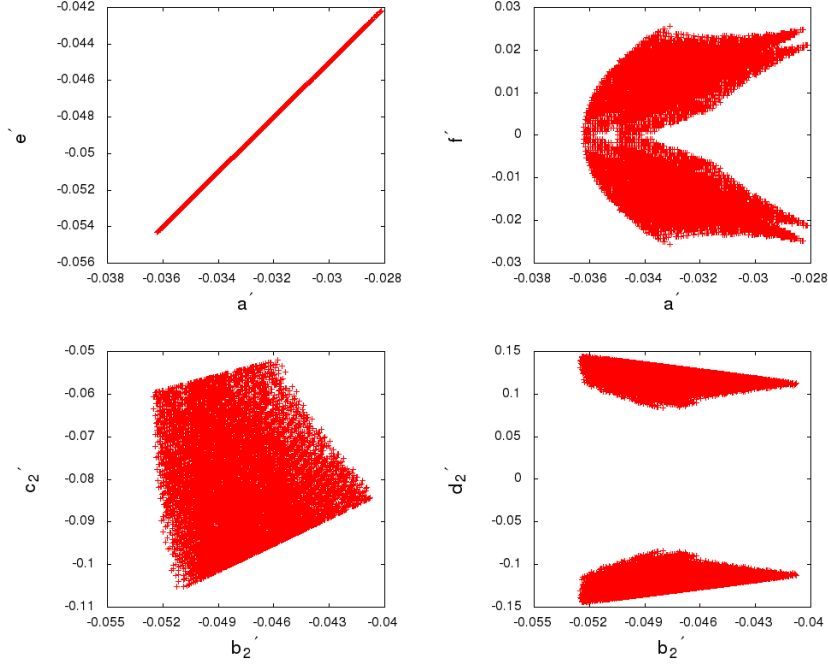


Figure 1: Case-I: Plots of the primed parameters for a normal mass hierarchy.

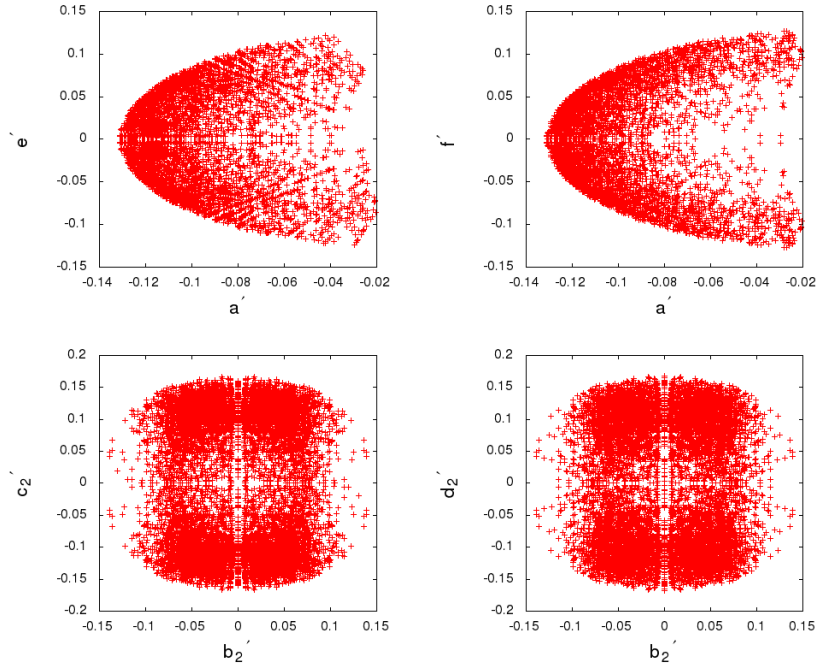


Figure 2: Case-I: Plots of the primed parameters for an inverted mass hierarchy.

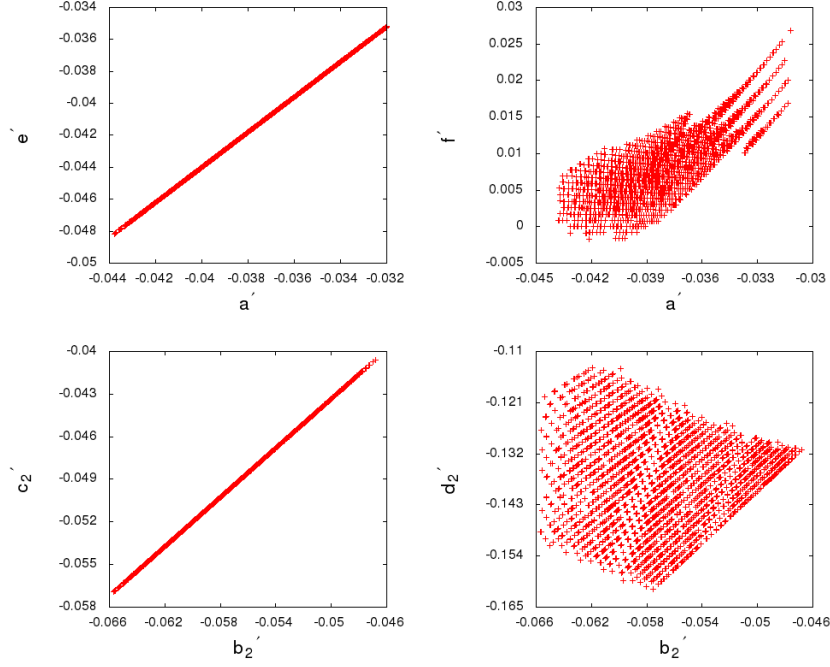


Figure 3: Case-II: Plots of the primed parameters for a normal mass hierarchy.

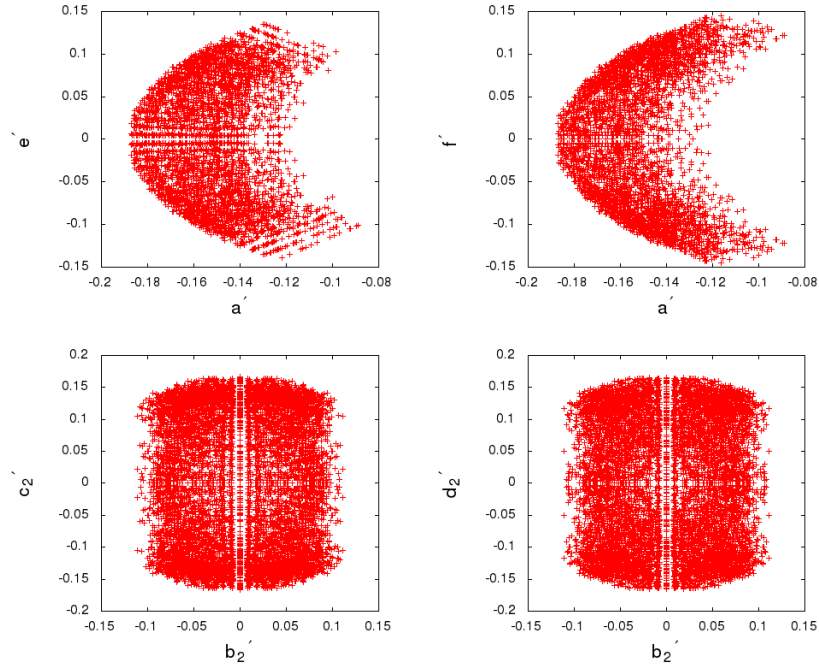


Figure 4: Case-II: Plots of the primed parameters for a normal mass hierarchy.

Table 3: Predictions on the light neutrino masses and $\sum_i m_i$.

Case-I					
Normal Ordering			Inverted Ordering		
$m_1/10^{-3}$ (eV)	$m_2/10^{-3}$ (eV)	$m_3/10^{-3}$ (eV)	$m_1/10^{-3}$ (eV)	$m_2/10^{-3}$ (eV)	$m_3/10^{-3}$ (eV)
4.0 – 8.5	9.28 – 12.0	49 – 52	47 – 61	49 – 62	9 – 36
$\sum_i m_i < 0.08$ eV			$\sum_i m_i < 0.16$ eV		
Case-II					
Normal Ordering			Inverted Ordering		
$m_1/10^{-3}$ (eV)	$m_2/10^{-3}$ (eV)	$m_3/10^{-3}$ (eV)	$m_1/10^{-3}$ (eV)	$m_2/10^{-3}$ (eV)	$m_3/10^{-3}$ (eV)
4.1 – 8.8	9.23 – 13.1	48 – 52	47 – 60	49 – 61	10 – 38
$\sum_i m_i < 0.08$ eV			$\sum_i m_i < 0.16$ eV		

Neutrinoless double beta decay ($\beta\beta_{0\nu}$)

This is a process arising from the decay of a nucleus as

$$(A, Z) \longrightarrow (A, Z + 2) + 2e^- \quad (5.2)$$

where the lepton number is violated by 2 units due to the absence of any final state neutrinos. Observation of such decay will lead to the confirmation of the Majorana nature of the neutrinos. The half-life [46] corresponding to the above decay is given by

$$\frac{1}{T_{1/2}^{0\nu}} = G|\mathcal{M}|^2|M_{ee}|^2m_e^{-2}, \quad (5.3)$$

where G is the two-body phase space factor, \mathcal{M} is the nuclear matrix element (NME), m_e is the mass of the electron and M_{ee} is the (1,1) element of the effective light neutrino mass matrix M_ν . Using the PDG parametrization convention for U_{PMNS} [28], the M_{ee} can be written as

$$M_{ee} = c_{12}^2 c_{13}^2 m_1 + s_{12}^2 c_{13}^2 m_2 e^{i\alpha} + s_{13}^2 m_3 e^{i(\beta-2\delta)}. \quad (5.4)$$

Significant upper limits on $|M_{ee}|$ are available from several ongoing experiments. Experiments such as KamLAND-Zen [48] and EXO [47] have constrained this value to be < 0.35 eV. However, till date the most impressive upper bound of 0.22 eV on $|M_{ee}|$ is provided by GERDA phase-I data [49] which is likely to be lowered even further by GERDA phase -II data [50] to around 0.098 eV. As shown in Ref. [30], existence of $G_3^{(k)}$ in the neutrino mass matrix leads to four sets of values of the CP-violating Majorana phases α and β for each neutrino mass ordering. Since $|M_{ee}|$ is sensitive to these phases, we get four different plots for each mass ordering. In Fig.5 we present the plots of $|M_{ee}|$ vs. the lightest neutrino mass ($m_{1,3}$) for both

the mass orderings in Case-I only. Apart from slight changes in the upper and lower limits on $m_{1,3}$, Case-II also leads to similar plots since it also predicts same results on CP violating phases (i.e. $\cos \delta = 0, \alpha, \beta = 0$ or π).

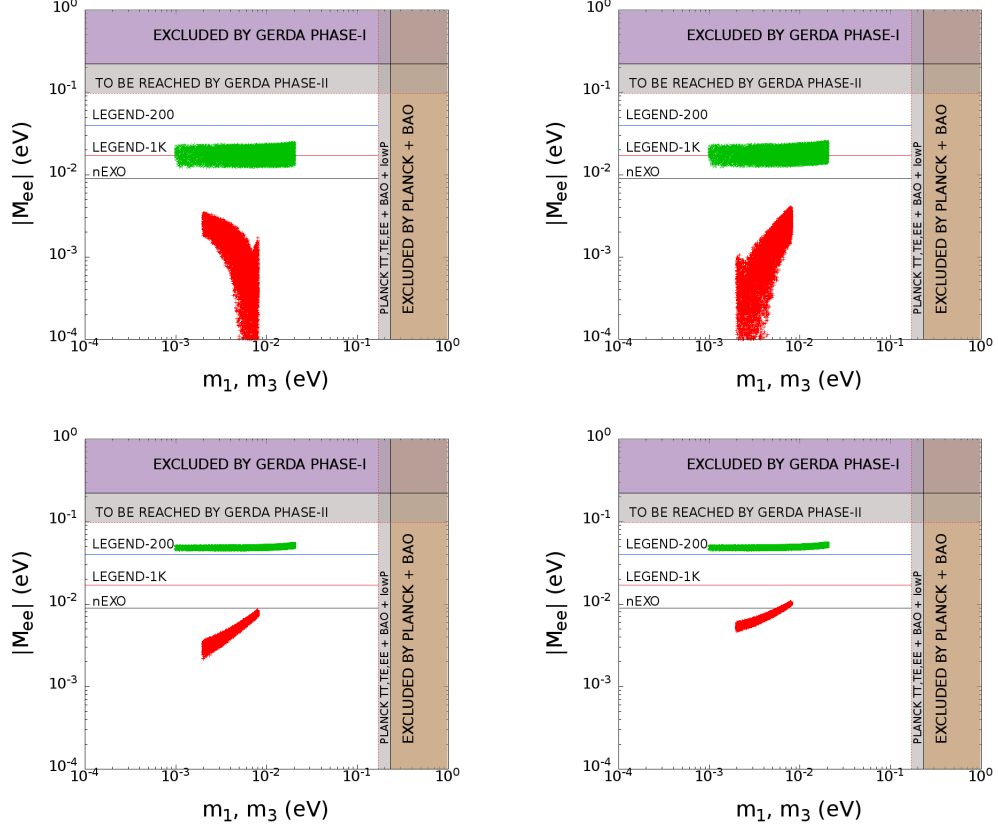


Figure 5: Plot of $|M_{ee}|$ vs. the lightest neutrino mass: the top two figures represent Case A: $\alpha = \pi$, $\beta = 0$ (left) and Case B: $\alpha = \pi$, $\beta = \pi$ (right) while the figures in the lower panel represent Case C: $\alpha = 0$, $\beta = 0$ (left) and Case D: $\alpha = 0$, $\beta = \pi$ (right).

This is evident from Fig.5 that $|M_{ee}|$ in each plot leads to an upper limit which is below the reach of the GERDA phase-II data. However, predictions of our model could be probed by GERDA + MAJORANA experiments [51]. Sensitivity reach of other promising experiments such as LEGEND-200 (40 meV), LEGEND-1K (17 meV) and nEXO (9 meV) [52] are also shown in Fig.5. Note that for each case, the entire parameter space corresponding to the inverted mass ordering could be ruled out by the nEXO reach. One can also explain the nature of the plots analytically. Let us first consider the inverted mass ordering. In this case, with the approximations $m_3 \simeq 0$ and $m_1 \simeq m_2$, $|M_{ee}|$ simplifies to

$$|M_{ee}| = \sqrt{|\Delta m_{32}|^2 c_{13}^2 [\{1 - s_{12}^2(1 - \cos \alpha)\}^2 + s_{12}^4 \sin^2 \alpha]^{1/2}}. \quad (5.5)$$

Clearly, $|M_{ee}|$ is not sensitive to the phases β and δ . On the other hand, for $\alpha = \pi$ and 0 (5.5)

further simplifies to

$$|M_{ee}| = \sqrt{|\Delta m_{32}|^2 c_{13}^2 \{1 - 2s_{12}^2\}^2} \quad (5.6)$$

and

$$|M_{ee}| = \sqrt{|\Delta m_{32}|^2 c_{13}^2} \quad (5.7)$$

respectively. Therefore, for $\alpha = \pi$ (cases A, B), $|M_{ee}|$ is suppressed as compared to the case $\alpha = 0$ (cases C, D). Now for a normal mass ordering, in addition to the s_{13} suppression, there is a significant interference between the first two terms. If $\alpha = 0$, the first two terms interfere constructively and we obtain a lower bound ($\sim 10^{-3}$ eV for Case C and $\sim 5 \times 10^{-3}$ eV for Case D) despite it being a case of normal mass ordering of the light neutrinos. This is one of the crucial results of the present analysis. On the other hand, for $\alpha = \pi$, the first two terms interfere destructively and thus a sizable cancellation between them brings down the value of $|M_{ee}|$ and results in the kinks that is depicted in the lower curves in the top two figures.

Baryogenesis via flavored leptogenesis

As mentioned in the beginning of the numerical section, to get a positive Y_B , we were obliged to use those value of the primed parameters for which the low energy neutrino parameters predicted from our model lie close to their best fit values dictated by the oscillation experiment. To facilitate this purpose, we define a variable χ^2 in Eq.(5.8) that measures the deviation of the parameters from their best fit values.

$$\chi^2 = \sum_{i=1}^5 \left[\frac{\mathcal{O}_i(th) - \mathcal{O}_i(bf)}{\Delta \mathcal{O}_i} \right]^2. \quad (5.8)$$

In Eq.(5.8)) \mathcal{O}_i denotes the i^{th} neutrino oscillation observable among $\Delta m_{21}^2, \Delta m_{32}^2, \theta_{12}, \theta_{23}$ and θ_{13} and the summation runs over all of them. The parenthetical *th* stands for the numerical value of the observable given by our model, whereas *bf* denotes the best fit value (cf. Table 2). $\Delta \mathcal{O}_i$ in the denominator stands for the measured 1σ range of \mathcal{O}_i . For numerical computation, we choose $M_{i+1}/M_i = 10^3$ ($i = 1, 2$)³. First we calculate χ^2 as a function of the primed parameters in their constrained range. For a fixed value of M_1 , we then start with the minimum value of χ^2 and we keep on increasing it until Y_B attains a positive value. For that particular χ^2 i.e., for a particular set of primed parameters, we are then able to generate a large set of unprimed parameters by varying M_1 over a wide range and can calculate Y_B for each value of M_1 . Let's discuss our results case by case for each mass ordering.

Case-I: Y_B for normal mass ordering of light neutrinos:

³In the next section a detailed discussion is given regarding the sensitivity of Y_B to the chosen hierarchy of M_i .

$M_1 < 10^9$ GeV: In this regime, all three lepton flavors (e, μ, τ) are distinguishable. Since $\varepsilon_1^e = 0$, we need to individually evaluate $\varepsilon_1^{\mu, \tau}$ only. Numerically, the maximum value of $|\varepsilon_1^{\mu, \tau}|$ is found to be $\sim 10^{-8}$. Y_B in the observed range cannot be generated with such a small CP asymmetry parameter. Theoretically, this can be understood as an interplay between various quantities. A unique feature in the present model is that the nonzero value of θ_{13} and ε_i originated from the imaginary part of the m_D matrix.

10^9 GeV $< M_1 < 10^{12}$ GeV: Before calculating final Y_B , we have to look first at the wash-out parameters $K_\alpha = \tilde{m}_\alpha/10^{-3}$ relevant to this mass regime. Since in this regime only τ flavor is distinguishable, there are two wash-out parameters, K_τ and $K_2 = K_e + K_\mu$. As shown in the first plot of Fig.6, the entire range of these parameters is not much greater than 1 for the observed range of Y_B . Thus the efficiency factor in Eq.(4.16) can be written for this mild wash-out scenario [39] as

$$\eta(\tilde{m}_\alpha) = \left[\left(\frac{\tilde{m}_\alpha}{8.25 \times 10^{-3}} \right)^{-1} + \left(\frac{0.2 \times 10^{-3}}{\tilde{m}_\alpha} \right)^{-1.16} \right]^{-1}. \quad (5.9)$$

We then perform a χ^2 scanning of the primed parameters. It has been found that for $\chi_{min}^2 = 0.083$ one can have Y_B positive. Basically, In our scheme, Eq.(4.16) of the present manuscript can be written as

$$Y_B \simeq \frac{12}{37g^*} \varepsilon_1^\mu \left[\eta \left(\frac{390}{589} \tilde{m}_\tau \right) - \eta \left(\frac{417}{589} \tilde{m}_2 \right) \right]. \quad (5.10)$$

Thus the sign of Y_B depends upon the sign of ε_1^μ and the sign of the bracketed quantity. Now from the primed parameter space we take a particular set, calculate the corresponding χ^2 and then compute Y_B . This has been seen that data sets corresponding to $\chi^2 < 0.083$ cannot produce positive Y_B , since for those data sets, we get positive values of ε_1^μ but negative values for the bracketed quantity. A complete data set of the primed parameters and corresponding values of the observables are tabulated in Table 4 for $\chi_{min}^2 = 0.083$. The other parameters i.e., b_1, c_1, d_1 can be calculated using Eq.(3.9)-(3.11).

Table 4: Parameters and observables corresponding $\chi^2 = 0.083$ for normal mass ordering.

a'	e'	f'	b'_2	c'_2	d'_2	χ^2
-0.036	-0.050	0.003	-0.052	-0.059	-0.122	0.083
observables	θ_{13}	θ_{12}	θ_{23}	$\Delta m_{21}^2 \times 10^5$	$ \Delta m_{31} ^2 \times 10^3$	
$\chi^2 = 0.083$	8.42^0	33.04^0	42.54^0	7.57 (eV) ²	2.55 (eV) ²	

Finally, given the primed data set for that χ_{min}^2 , M_1 is varied widely to have Y_B in the observed range. For each value of M_1 , a set of values of the unprimed parameters

$\{a, e, f, b_1, c_1, d_1, b_2, c_2, d_2\}$ is generated. Final Y_B is then calculated for each values of M_1 and the corresponding unprimed set. A careful surveillance of the plot in Fig.7 leads to the conclusion that we can obtain an upper and a lower bound on M_1 due to the observed constraint on Y_B . In order to appreciate this fact more clearly, two straight lines have been drawn parallel to the abscissa in the mentioned plot: one at $Y_B = 8.55 \times 10^{-11}$ and the other at $Y_B = 8.77 \times 10^{-11}$. The values of M_1 , where the straight lines meet the Y_B vs M_1 curve, yield the allowed lower and upper bounds on M_1 , namely $(M_1)_{lower} = 2.17 \times 10^{11}$ GeV and $(M_1)_{upper} = 2.23 \times 10^{11}$ GeV. To explain this linear correlation between M_1 and Y_B one could see the expression for ε_1^μ in Eq.(6.1). As we see from Eq.(6.1), ε_1^α is composed of two terms. The first term is proportional to M_1/M_j while the second term is proportional $(M_1/M_j)^2$. Now for the assumed hierarchical scenario ($M_3 \gg M_2 \gg M_1$), the first term dominates (cf. Eq.6.2) and effectively ε_1^α becomes proportional to M_1 (theoretically which is not the case due to the presence of the second term). Now in Eq.(4.16), in the expression of Y_B , the wash-out parameters only depend upon the primed parameters. Thus effectively the final baryon asymmetry Y_B is also proportional to M_1 . One might also ask about the narrow range for M_1 as we see in the Fig.7. Basically we have presented our result for a particular set of primed parameters (for $\chi^2_{min} = 0.083$). In principle one can take the entire primed parameter space of our model and compute the corresponding results on Y_B and M_1 for each set of primed parameters. In that case (for the entire parameter space) the range of M_1 should not be as narrow as we see in this case.

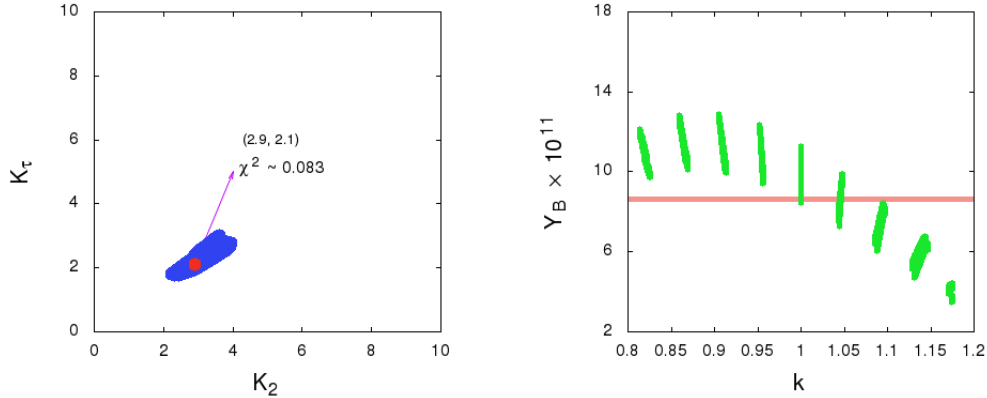


Figure 6: The plot on the left hand side shows the range of the wash-out parameters. The red dot corresponds to the minimum value of χ^2 for which a set of primed parameters has been taken to compute Y_B . The plot on the right hand side shows a variation of Y_B vs k . The red band in the same plot indicates the observed range of Y_B .

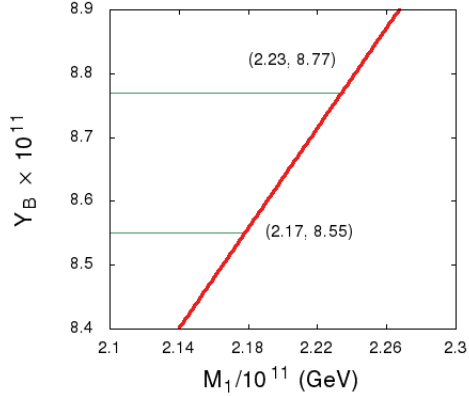


Figure 7: A plot of the final Y_B for different values of M_1 for a normal light neutrino mass ordering.

From Table 4, we infer that $\theta_{23} = 42.54^0$ corresponding to $\chi_{min}^2 = 0.083$. Since theoretically θ_{23} is related only with a single model parameter k (cf. Eq.(2.20)) and unlike the other parameters of m_D (discussed earlier in this section) value of k does not depend upon the variation of M_1 , θ_{23} remain fixed for the entire range of M_1 that corresponds to the observed range of Y_B . Thus an experimentally appealing conclusion of this scheme is that, given the observed range of Y_B , the octant of θ_{23} is determined ($< 45^0$). One can also check the sensitivity of the produced Y_B to the entire range of θ_{23} in a slightly different way. It is trivial to find out the analytic form of Y_B that explicitly depend upon θ_{23} , by replacing $k = (\tan \theta_{23})^{-1}$ in the expression of ε_1^μ and m_α in Eq.(5.10). Thus for a fixed value of M_1 one can use the entire parameter space of the primed parameters and k to compute the final Y_B . From the plot on the right panel of Fig.6, we see that the value of k is always greater than 1 for Y_B to be in the observed range (represented by the red narrow strip in Fig.6). This is certainly for a particular value of $M_1 (6.79 \times 10^{11} \text{ GeV})$. As previously mentioned, Y_B is almost proportional to M_1 , thus lowering the value of the latter below $6.79 \times 10^{11} \text{ GeV}$ would cause a downward movement of the overall pattern of the Y_B vs. k plot in Fig.6. Thus for the observed range of Y_B , along with the values $k > 1$, there would be other values of k which are less than one. It is seen that for the normal mass ordering in Case-II a similar lower limit on M_1 exist that dictates the octant of θ_{23} for the the observed range of Y_B .

We would like to stress that the lower bound obtained in the second approach is different from that is obtained in the first one. This is simply because the ways to obtain these bounds are different. In the first approach we take the best fit values of the primed parameters and k and then vary M_1 to obtain the observed range of Y_B which in turn leads to an upper and a lower bound on M_1 . However, in the second approach, we take the entire primed parameter space along with the allowed range for k and then compute Y_B for a fixed value of M_1 . The Y_B vs. k plot in Fig.6 is for $M_1 = 6.79 \times 10^{11} \text{ GeV}$ which represents the lower bound on M_1 above

which we always get $k > 1$ for the observed range of Y_B . Now what happens if we further lower the value of M_1 from 6.79×10^{11} GeV in the second approach? As discussed previously, this would imply a downward movement of Y_B vs k curve in Fig.6 or in Fig.9. In that case both $k > 1$ and $k < 1$ values are possible for the observed range of Y_B . Obviously this has an impact on the results obtained in the first method. We know from the first method that if we choose the best fit value of k , the allowed range of M_1 should be read from Fig.7. This does not necessarily mean that for this range of M_1 , other values of k are not possible (obviously those values of k should not be the best fit values then) since the range shown in Fig.7 is below $M_1 = 6.79 \times 10^{11}$ GeV.

$M_1 > 10^{12}$ GeV: It has been shown that $Y_B = 0$ here for our model.

Case-I: Y_B for inverted mass ordering of light neutrinos:

Following the same procedure as for the normal mass ordering, a final discussion for each regime is summarized as follows.

$M_1 < 10^9$ GeV: Similar to the normal ordering, the $|\varepsilon_1^{\mu,\tau}|$ can have values at most the order of 10^{-8} which is not sufficient to let Y_B come within its observed range.

10^9 GeV $< M_1 < 10^{12}$ GeV: Unlike the previous case the ranges of the the wash-out parameters (cf. Fig.8) favors a strong wash-out scenario.

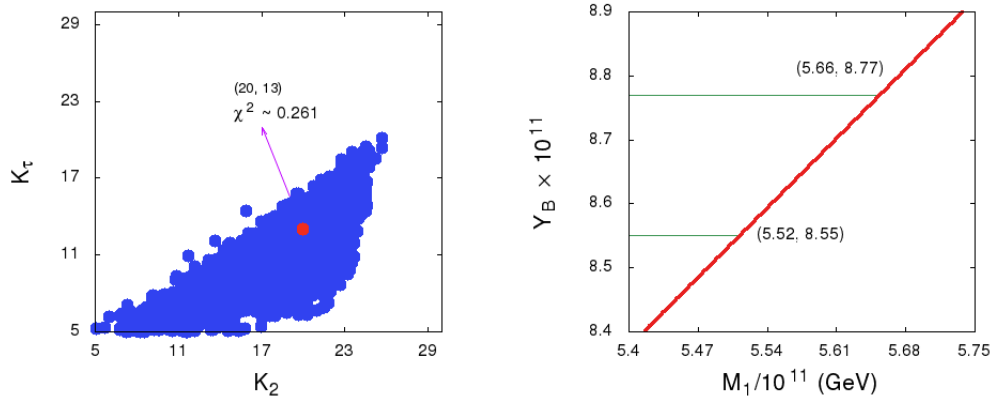


Figure 8: The plot on the left hand side shows the range of the wash-out parameters. The red dot corresponds to the minimum value of χ^2 for which a set of primed parameter has been taken to compute Y_B . The plot on the right hand side shows final Y_B for different values of M_1 for the inverted light neutrino mass ordering.

Thus the efficiency factor in Eq.(4.16) can be written for this strong wash-out scenario [39] as

$$\eta(\tilde{m}_\alpha) = \left[\left(\frac{0.55 \times 10^{-3}}{\tilde{m}_\alpha} \right)^{1.16} \right]. \quad (5.11)$$

For $\chi^2_{min} = 0.261$, a set of primed parameters is obtained (cf. Table 5). Then similar to the previous case, varying M_1 in a wide range, a lower and upper bound on M_1 , namely $(M_1)_{lower} = 5.52 \times 10^{11}$ GeV and $(M_1)_{upper} = 5.66 \times 10^{11}$ GeV is obtained for the observed range of Y_B . A plot of Y_B vs M_1 is shown in the right panel of Fig.8.

Table 5: Parameters and observables corresponding $\chi^2 = 0.261$ for inverted hierarchy.

a'	e'	f'	b'_2	c'_2	d'_2	χ^2
-0.043	-0.065	0.116	0.130	-0.019	0.039	0.261
observables	θ_{13}	θ_{12}	θ_{23}	$\Delta m_{21}^2 \times 10^5$	$ \Delta m_{31} ^2 \times 10^3$	
$\chi^2 = 0.261$	8.54^0	34.07^0	49.37^0	7.53 (eV)^2	2.40 (eV)^2	

$M_1 > 10^{12}$ GeV: Once again, $Y_B = 0$ in this regime, for the present model.

Case-II: Y_B for normal mass ordering of light neutrinos:

The analysis has been done exactly in the same way as was in the previous case. A systematic presentation of the obtained results is the following.

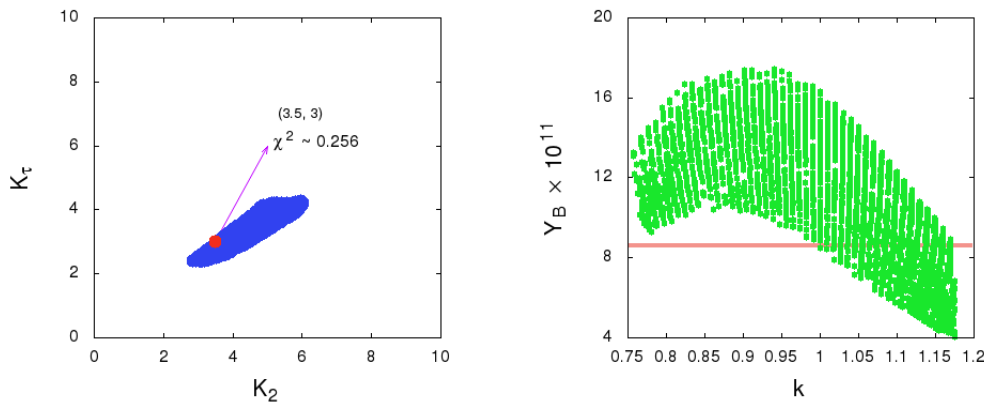


Figure 9: The plot on the left hand side shows the range of the wash-out parameters. The red dot corresponds to the minimum value of χ^2 for which a set of primed parameter has been taken to compute Y_B . The plot on the right hand side shows a variation of Y_B vs k . The red band in the same plot indicates the observed range of Y_B .

$M_1 < 10^9$ GeV: Again, Y_B in the observed range cannot be generated due to the small value of $|\varepsilon_1^{\mu,\tau}|$.

10^9 GeV $< M_1 < 10^{12}$ GeV: Similar to the previous normal hierarchical case, the wash-out parameters here also suggest a mild wash-out scenario (cf. Fig.9).

For $\chi_{min}^2 = 0.256$, a set of rescale parameter has been found and then varying M_1 in a wide range, a lower and an upper bound on M_1 are obtained as shown in the Fig.10. Note that in this case also $\theta_{23} < 45^\circ$ (Table 6) for the minimum χ^2 that produce Y_B positive and in the observed range. Similar to the case of normal mass ordering in Case-I, here we also show a Y_B vs k plot (cf. Fig.9) and infer that there exists a lower limit 8.2×10^{11} GeV on M_1 for which $k > 1$, i.e., $\theta_{23} < 45^\circ$ for Y_B to be in the observed range.

Table 6: Parameters and observables corresponding $\chi^2 = 0.256$ for normal mass ordering.

a'	e'	f'	b'_2	c'_2	d'_2	χ^2
-0.042	-0.046	-0.005	-0.065	-0.056	-0.128	0.256
observables	θ_{13}	θ_{12}	θ_{23}	$\Delta m_{21}^2 \times 10^5$	$ \Delta m_{31} ^2 \times 10^3$	
$\chi^2 = 0.256$	8.37°	33.08°	43.49°	7.55 (eV) 2	2.55 (eV) 2	

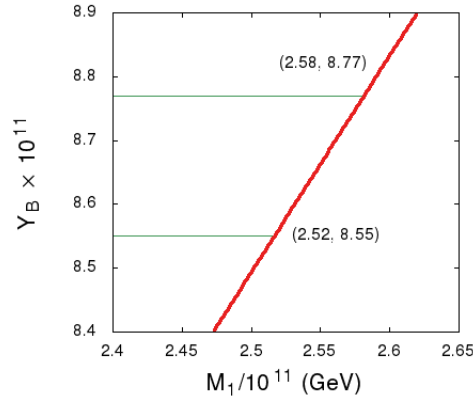


Figure 10: A plot of the final Y_B for different values of M_1 for the normal light neutrino mass ordering.

$M_1 > 10^{12}$ GeV: It has been shown that $Y_B = 0$ here for our model.

Case-II: Y_B for inverted mass ordering of light neutrinos:

Proceeding exactly in the same manner as for the normal mass ordering, a brief discussion for each regime goes as follows.

$M_1 < 10^9$ GeV: Similar to the normal ordering, the $|\varepsilon_1^{\mu,\tau}|$ can have values at most the order of 10^{-8} which is not sufficient to let Y_B come within its observed range.

10^9 GeV $< M_1 < 10^{12}$ GeV: Unlike the previous case the ranges of the wash-out parameters (cf. Fig.11) favors a strong wash-out scenario. For $\chi^2_{min} = 0.041$ a set of primed parameters is obtained (cf Table 7). Then similar to the previous case varying M_1 in a wide range a lower and upper bound on M_1 , namely $(M_1)_{lower} = 5.27 \times 10^{11}$ GeV and $(M_1)_{upper} = 5.40 \times 10^{11}$ GeV is obtained for the observed range of Y_B . A plot of Y_B vs M_1 is shown in the right panel of Fig.11.

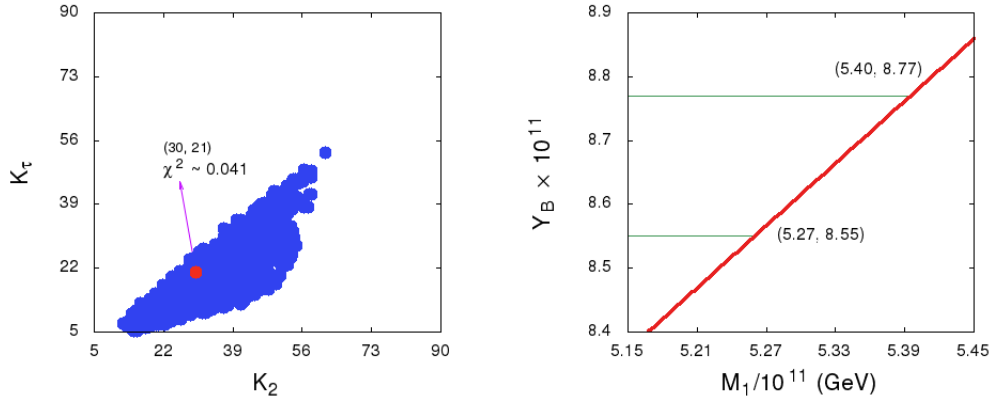


Figure 11: The plot on the left hand side shows the range of the wash-out parameters. The red dot corresponds to the minimum value of χ^2 for which a set of primed parameter has been taken to compute Y_B . The plot on the right hand side shows final Y_B for different values of M_1 for the inverted light neutrino mass ordering.

Table 7: Parameters and observables corresponding $\chi^2 = 0.041$ for inverted hierarchy.

a'	e'	f'	b'_2	c'_2	d'_2	χ^2
-0.123	-0.084	0.123	0.104	-0.052	-0.096	0.041
observables	θ_{13}	θ_{12}	θ_{23}	$\Delta m_{21}^2 \times 10^5$	$ \Delta m_{31} ^2 \times 10^3$	
$\chi^2 = 0.041$	8.71^0	33.43^0	49.23^0	7.58 (eV) ²	2.44 (eV) ²	

$M_1 > 10^{12}$ GeV: Once again, $Y_B = 0$ here for the present model.

A compact presentation of the final conclusions regarding Y_B from the numerical analysis is given in Table 8.

Table 8: Final statements on Y_B for different mass regimes.

Case-I			
Type	$M_1 < 10^9$ GeV	10^9 GeV $< M_1 < 10^{12}$ GeV	$M_1 > 10^{12}$ GeV
Normal Ordering	Ruled out since Y_B is below the observed range for any χ^2 .	Y_B within the observed range for $\chi_{min}^2 = 0.083$.	Ruled out since $Y_B = 0$.
Inverted Ordering	Ruled out since Y_B is below the observed range for any χ^2 .	Y_B within the observed range for $\chi_{min}^2 = 0.261$.	Ruled out since $Y_B = 0$.
Case-II			
Type	$M_1 < 10^9$ GeV	10^9 GeV $< M_1 < 10^{12}$ GeV	$M_1 > 10^{12}$ GeV
Normal Ordering	Ruled out since Y_B is below the observed range for any χ^2 .	Y_B within the observed range for $\chi_{min}^2 = 0.256$.	Ruled out since $Y_B = 0$.
Inverted Ordering	Ruled out since Y_B is below the observed range for any χ^2 .	Y_B within the observed range for $\chi_{min}^2 = 0.041$.	Ruled out since $Y_B = 0$.

Before concluding this section we want to stress the following point. In this model, the imaginary part of m_D^{MS} of Eq.(3.8) plays a crucial role. Absence of the latter leads to a vanishing θ_{13} , and thus undetermined value of δ and most importantly a vanishing value of ε_i^α . Thus the model addresses a common origin of θ_{13} , CP violation and leptogenesis. However, although the parameters in the imaginary part of m_D^{MS} are correlated with Y_B , from Eq.(4.7) we see the parameter b_1 is also very much sensitive to ε_1^α . For example, for $b_2 = 0$ and $c_2, d_2 \neq 0$, Eq.(4.7) is simplified as

$$\varepsilon_1^\mu = 4\pi v^2 [b_1^2 + (a^2 + b_1^2)k^2]^{-1} b_1 \chi_4 = -\varepsilon_1^\tau, \quad (5.12)$$

where $\chi_4 = f(c_2, d_2)$ as defined in Eq.(4.12). Now if b_1 vanishes ε_1^μ , hence, Y_B vanishes but due to nonvanishing value of c_2, d_2 one obtains $\theta_{13} \neq 0$. However, to obtain a nonzero Y_B , along with a nonvanishing b_1 , one always needs $\chi_4 \neq 0$ which in turn implies a nonzero θ_{13} . Thus in this model a nonzero θ_{13} does not always imply a nonzero Y_B but the reverse is not true.

6 Effect of $N_{2,3}$ on Y_B

In our analysis, the effect of the two heavier neutrinos (N_2, N_3) on the produced final baryon asymmetry has been neglected with the assumption that the asymmetries produced by the

decays of both of them get washed out [37]. In this section, we present a brief discussion on the sensitivity of the heavier neutrinos to final Y_B . There are two ways that such a sensitivity might arise as elaborated below.

Indirect effect of $N_{2,3}$:

Though the neutrino oscillation data are fitted with the primed parameters, cf Eq.(5.1), for computing the quantities related to leptogenesis, e.g., ε_1^α , we need to evaluate the unprimed ones, i.e. the Dirac mass matrix elements. It is interesting to see whether the final baryon asymmetry is affected by the chosen hierarchies of the RH neutrinos. We find that the final Y_B is not much sensitive to $M_{2,3}$. One can appreciate this statement by simplifying the CP asymmetry parameters of Eq.(4.2) to

$$\varepsilon_1^\alpha = -\frac{3}{8\pi v^2 h_{11}} \sum_{j=2,3} \frac{M_1}{M_j} \text{Im}[h_{1j}(m_D)_{1\alpha}(m_D^*)_{j\alpha}] - \frac{1}{4\pi v^2 h_{11}} \sum_{j=2,3} \frac{M_1^2}{M_j^2} \text{Im}[h_{j1}(m_D)_{1\alpha}(m_D^*)_{j\alpha}] \quad (6.1)$$

after approximating $g(x_{1j})$ of Eqs.(4.3) to $g(x_{1j}) = -\frac{3}{2\sqrt{x_{1j}}}$ for $x_{1j} \gg 1$. The last term of Eq.(6.1) is suppressed because it is of second order in x_{1j}^{-1} . Having two parts for $j = 2, 3$, $j = 3$ term of the first term of Eq.(6.1) has a negligible effect on ε_1^α since M_3 is much larger than M_1 and f, d_1 and d_2 have values of the order of the other Dirac components. Now for $j = 2$, ε_1^α is simplified as

$$\varepsilon_1^\mu = -\frac{3M_1}{8\pi v^2 h_{11}} [(ae' + b_1c'_1 + b_2c'_2)(b_2c'_1 + b_1c'_2)] = -\varepsilon_1^\tau \quad (6.2)$$

with $\varepsilon_1^e = 0$ as already shown in Sec.4. Since the primed parameters are fixed by the oscillation data, $\varepsilon_1^{\mu,\tau}$ are practically insensitive to the value of M_2 . However, for the numerical computation of the final baryon asymmetry, we take into account each term in Eq.(6.1) with two different mass hierarchical schemes for the heavy neutrinos, e.g, $M_{i+1}/M_i = 10^2$ and $M_{i+1}/M_i = 10^4$ where i can take the values 1, 2. Note that in the previous section we have already computed Y_B for $M_{i+1}/M_i = 10^3$. The outcome of the numerical analysis is that though the chosen mass ratios of the RH neutrinos are altered, changes in the lower and upper bounds on M_1 are not significant for the observed range of Y_B . For convenience, for each case and light neutrino mass ordering, the variation of Y_B with M_1 for different mass ratios has been presented in Table 9.

Table 9: Lower and upper bounds on M_1 for different mass ratios of the RH neutrinos ($i = 1, 2$).

Case-I: Normal light neutrino ordering			
Hierarchies \rightarrow	$M_{i+1}/M_i = 10^2$	$M_{i+1}/M_i = 10^3$	$M_{i+1}/M_i = 10^4$
Upper bound (GeV)	2.21×10^{11}	2.23×10^{11}	2.25×10^{11}
Lower bound (GeV)	2.16×10^{11}	2.17×10^{11}	2.18×10^{11}
Case-I: Inverted light neutrino ordering			
Hierarchies \rightarrow	$M_{i+1}/M_i = 10^2$	$M_{i+1}/M_i = 10^3$	$M_{i+1}/M_i = 10^4$
Upper bound (GeV)	5.64×10^{11}	5.66×10^{11}	5.67×10^{11}
Lower bound (GeV)	5.51×10^{11}	5.52×10^{11}	5.54×10^{11}
Case-II: Normal light neutrino ordering			
Hierarchies \rightarrow	$M_{i+1}/M_i = 10^2$	$M_{i+1}/M_i = 10^3$	$M_{i+1}/M_i = 10^4$
Upper bound (GeV)	2.57×10^{11}	2.58×10^{11}	2.59×10^{11}
Lower bound (GeV)	2.50×10^{11}	2.52×10^{11}	2.54×10^{11}
Case-II: Inverted light neutrino ordering			
Hierarchies \rightarrow	$M_{i+1}/M_i = 10^2$	$M_{i+1}/M_i = 10^3$	$M_{i+1}/M_i = 10^4$
Upper bound (GeV)	5.38×10^{11}	5.40×10^{11}	5.42×10^{11}
Lower bound (GeV)	5.25×10^{11}	5.27×10^{11}	5.28×10^{11}

One can see from Table 9 that the lower and upper bounds on M_1 slightly differ in each hierarchical cases. As explained before, the first term in Eq.(6.1) is not sensitive to the chosen hierarchies. However, the second term contributes to the ε_1^μ and hence to the final Y_B . Thus for the same value of M_1 , contribution from the second term in Eq.(6.1) is larger for $M_{i+1}/M_i = 10^2$ and smaller for $M_{i+1}/M_i = 10^4$ compare to $M_{i+1}/M_i = 10^3$ case. Hence for $M_{i+1}/M_i = 10^2$ case, slope of the Y_B Vs. M_1 curve is larger than the case of $M_{i+1}/M_i = 10^3$. Consequently both upper and the lower bounds get slightly lowered (compared to standard $M_{i+1}/M_i = 10^3$ case) for the given range of Y_B . Proceeding in the same way we obtain a little bit increased bounds for $M_{i+1}/M_i = 10^4$ case.

Direct effect of N_2 :

For simplicity, here we consider only the effect of N_2 . It is shown in Ref. [38] that, due to a decoherence effect, a finite amount of lepton asymmetry generated by N_2 decays get protected against N_1 -washout thus survive down to the electroweak scale and contribute to the final

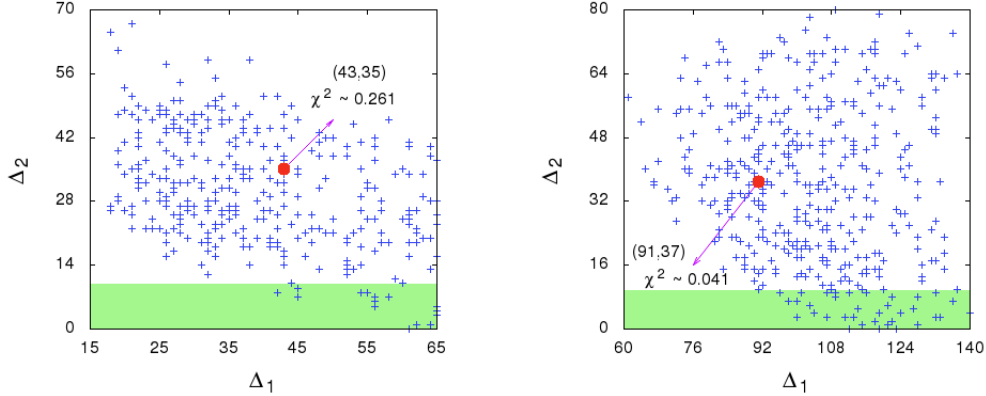


Figure 12: Plots of the wash-out parameters Δ_1 and Δ_2 for inverted light neutrino mass ordering for both the cases. The red dot corresponds to the corresponding χ^2_{min} for which we calculate the final baryon asymmetry.

baryon asymmetry. For this procedure to happen, two wash-out parameters $\Delta_1 = \frac{h_{11}}{M_1 m^*}$ and $\Delta_2 = \frac{h_{22}}{M_2 m^*}$ must satisfy the condition $\Delta_1 \gg 1$ and $\Delta_2 \gg 1$ with $m^* = 1.66\sqrt{g^*}\pi v^2/M_{Pl} \approx 10^{-3}$ eV. Here $\Delta_1 \gg 1$ indicates that faster N_1 interactions destroy coherence among the states produced by N_2 , thus a part of the lepton asymmetry produced by N_2 survives orthogonal to N_1 -states and gets protected against N_1 -washout. On the other hand, a mild wash-out of the lepton asymmetry produced by N_2 due to N_2 -related interactions is represented by $\Delta_2 \gg 1$ condition. For this mild wash-out scenario, a sizable N_2 -generated lepton asymmetry survives during the N_1 -leptogenesis phase. It has been found that for each of the discussed cases, for a normal light neutrino mass ordering, both the wash-out parameters $\Delta_{1,2} < 10$. Thus faster N_1 interaction do not take place and condition for N_2 leptogenesis is violated. On the other hand for inverted light neutrino mass orderings, the allowed parametric region prefers large values of Δ_2 in excess of 10 except at the bottom (green band). Thus the $\Delta_2 \gg 1$ condition is violated in most of the region. Moreover the χ^2_{min} values, for which we calculate final Y_B strongly violates $\Delta_2 \gg 1$ condition. Few allowed points with $\Delta_2 < 10$ correspond to values of χ^2 above 0.8 which is much higher than χ^2_{min} for which we obtain Y_B in the observed range. Therefore, for our calculation, any direct effect of N_2 is not significant. Note that 0.8 is not a special value. What we are trying to address, is that there are some data points in the model parameter space for which the conditions for N_2 leptogenesis is satisfied. However, the minimum value of χ^2 for those data sets is 0.8. This means the corresponding observables are much away from their best-fit values. Practically every data point in the parameter space is acceptable if they produce Y_B in the observed range. However, throughout the analysis, for the computation of Y_B , we restrict ourselves close to the best fitted values. In that sense the data points which are away from the best fit values are disfavored.

7 Summary and conclusion

We present the Strong Scaling Ansatz (SSA) as a residual $\mathbb{Z}_2 \times \mathbb{Z}_2$ symmetry. Since SSA predicts a vanishing θ_{13} —thus no Dirac CP violation, we modify SSA with a complex extension of the residual $\mathbb{Z}_2 \times \mathbb{Z}_2$ by invoking a nonstandard CP transformation and address the new symmetry as a generalized $\mathbb{Z}_2 \times \mathbb{Z}_2$ symmetry. Depending upon the implementation of the symmetry, there are several cases that have been explored in this model. For each of the cases, besides the predictions of maximal Dirac CP violation ($\delta = \pm\pi/2$) and CP conserving values for the Majorana phases ($\alpha, \beta = 0, \pi$), constrained ranges for the $\beta\beta 0\nu$ decay parameter $|M_{ee}|$ and the light neutrino masses are also found. In this extended SSA, both the neutrino mass orderings are found to be allowed with upper bounds on $\sum_i m_i$ that are much lower than the present value 0.23 eV.

We further discuss the generalized $\mathbb{Z}_2 \times \mathbb{Z}_2$ within the framework of type-I seesaw mechanism. Baryogenesis via leptogenesis scenario has been explored qualitatively as well as quantitatively. Typical structure of the Dirac mass matrix m_D leads to a common origin of θ_{13} , leptonic CP violation and nonzero CP asymmetry parameter ε_i^α . Here we focus the N_1 -leptogenesis scenario as the primary one. However, we also discuss the effect of the heavier neutrinos $N_{2,3}$ on the final baryon asymmetry Y_B . It is shown that the heavier neutrinos might effect the final Y_B in two ways i) via the chosen hierarchy of the RH neutrinos and ii) through the asymmetry generated by the heavy neutrino itself (for simplicity we have assumed only the effect of N_2 , i.e., N_2 leptogenesis). We found that the final Y_B is not sensitive to the chosen hierarchy of the RH neutrinos since the leading order term in ε_1^α is independent of the chosen hierarchy. Throughout the analysis we restrict ourselves to the near best-fit values of the oscillation parameters for which a positive value of Y_B is obtained. We found that the conditions for N_2 leptogenesis are not satisfied for those best-fit points. Thus N_2 -leptogenesis is also not so sensitive to the final Y_B . For each of the cases and irrespective of the light neutrino mass ordering, only τ -flavored leptogenesis scenario ($10^9 \text{ GeV} < T \sim M_1 < 10^{12} \text{ GeV}$) is found to be feasible one to generate Y_B in the observed range with the other regimes $T \sim M_1 > 10^{12}$ and $T \sim M_1 < 10^9 \text{ GeV}$ being ruled out analytically as well as numerically. The best-fit parameters for which we calculate the final Y_B , lead to the value of $\theta_{23} < 45^\circ$ for normal mass orderings and $\theta_{23} > 45^\circ$ for inverted mass orderings for both Case-I and Case-II. We also found an upper and a lower bound on the lightest (M_1) of the heavy neutrino masses for each case. Finally for a fixed value of M_1 we also investigate θ_{23} sensitivity of the final Y_B . Although both the light neutrino mass orderings are allowed, the normal mass ordering comes up with an interesting prediction. It has been shown and explained in Sec.5 that in both the normal mass ordering scenarios, there exist lower limits on M_1 , above which any value of M_1 corresponds to $\theta_{23} < 45^\circ$ for Y_B to be in the observed range.

As a final note, the predictions of this model—thus the viability of modification to SSA

with a generalized $\mathbb{Z}_2 \times \mathbb{Z}_2$ symmetry, would be tested in the ongoing experiments such as GERDA-II [50], T2K [53], NO ν A [54] etc. shortly.

Acknowledgment

The work of the authors are supported by the the Department of Atomic Energy (DAE), Government of India. The authors would like to thank Probir Roy for discussion about residual symmetry. R. Samanta would like to thank Walter Grimus for a valuable discussion on CP transformation during a visit at the University of Vienna.

References

- [1] C.S Lam, Phys. Lett B **656**, 193 (2007); Phys. Rev. Lett. **101**, 121602 (2008); Phys. Rev. D **78**, 073015 (2008).
- [2] D. A. Dicus, S. F. Ge and W. W. Repko, Phys. Rev. D **83**, 093007 (2011), Phys. Lett. B **702**, 220 (2011), Phys. Rev. Lett. **108**, 041801 (2012). Hong-Jian He and Fu-Rong Yin, Phys. Rev. D **84** (2011) 033009. S.-F. Ge, Hong-Jian He, Fu-Rong Yin, JCAP 1005 (2010) **017**.
- [3] P. Byakti and P. B. Pal, [arXiv:1601.08063](https://arxiv.org/abs/1601.08063) [hep-ph].
- [4] C. S. Lam, Phys. Rev. D **89**, no. 9, 095017 (2014), B. Bajc and A. Y. Smirnov, Nucl. Phys. B **909**, 954 (2016).
- [5] W. Grimus and L. Lavoura, Acta Phys. Polon. B **34**, 5393 (2003); Phys. Lett. B 579, 113 (2004); Fortsch. der Phys. **61**, 535 (2013).
- [6] S. Gupta, A. S. Joshipura and K. M. Patel, Phys. Rev. D **85**, 031903 (2012)
- [7] L. Lavoura, Phys. Rev. D **62**, 093011 (2000). R. N. Mohapatra and W. Rodejohann, Phys. Lett. B **644**. 59 (2007).
- [8] A. S. Joshipura and W. Rodejohann, Phys. Lett. B **678**, 276 (2009). A. Ghosal and R. Samanta, JHEP **1505**, 077 (2015), R. Samanta, M. Chakraborty and A. Ghosal, Nucl. Phys. B **904**, 86 (2016). A. Blum, R. N. Mohapatra and W. Rodejohann, Phys. Rev. D **76**, 053003 (2007).
- [9] F. P. An *et al.* [Daya Bay Collaboration], Phys. Rev. Lett. **115**, 111802 (2015).
- [10] F. Feruglio, C. Hagedorn and R. Ziegler, JHEP **1307**, 027 (2013).
- [11] M. Holthausen, M. Lindner and M. A. Schmidt, JHEP **1304**, 122 (2013).

- [12] M. C. Chen, M. Fallbacher, K. T. Mahanthappa, M. Ratz and A. Trautner, Nucl. Phys. B **883**, 267 (2014).
- [13] S. F. King, Prog. Part. Nucl. Phys. **94**, 217 (2017).
- [14] G. J. Ding, S. F. King, C. Luhn and A. J. Stuart, JHEP **1305**, 084 (2013), F. Feruglio, C. Hagedorn and R. Ziegler, Eur. Phys. J. C **74**, 2753 (2014), G. J. Ding, S. F. King and A. J. Stuart, JHEP **1312**, 006 (2013).
- [15] C. C. Li and G. J. Ding, Nucl. Phys. B **881**, 206 (2014).
- [16] R. N. Mohapatra and C. C. Nishi, JHEP **1508**, 092 (2015).
- [17] C. C. Nishi and B. L. Sanchez-Vega, JHEP **1701**, 068 (2017).
- [18] Hong-Jian He and Xun-Jie Xu Phys. Rev. D **86** (2012) 111301.
- [19] Y. Koide, H. Nishiura, K. Matsuda, T. Kikuchi and T. Fukuyama, Phys. Rev. D **66**, 093006 (2002), W. Grimus, A. S. Joshipura, S. Kaneko, L. Lavoura, H. Sawanaka and M. Tanimoto, Nucl. Phys. B **713**, 151 (2005).
- [20] A. Ghosal and D. Majumdar, Phys. Rev. D **66**, 053004 (2002).
- [21] W. Grimus, A. S. Joshipura, S. Kaneko, L. Lavoura and M. Tanimoto, JHEP **0407**, 078 (2004), C. Hagedorn and W. Rodejohann, JHEP **0507**, 034 (2005), M. Honda, R. Takahashi and M. Tanimoto, JHEP **0601**, 042 (2006).
- [22] S. Pakvasa and H. Sugawara, Phys. Lett. **82B**, 105 (1979), Y. Cai and H. B. Yu, Phys. Rev. D **74**, 115005 (2006), Y. Koide, JHEP **0708**, 086 (2007). C. Hagedorn, M. Lindner and R. N. Mohapatra, JHEP **0606**, 042 (2006).
- [23] E. Ma and G. Rajasekaran, Phys. Rev. D **64**, 113012 (2001), G. Altarelli and F. Feruglio, Nucl. Phys. B **720**, 64 (2005) X. G. He, Y. Y. Keum and R. R. Volkas, JHEP **0604**, 039 (2006), B. Adhikary, B. Brahmachari, A. Ghosal, E. Ma and M. K. Parida, Phys. Lett. B **638**, 345 (2006).
- [24] G. C. Branco, J. M. Gerard and W. Grimus, Phys. Lett. **136B**, 383 (1984), E. Ma, Mod. Phys. Lett. A **21**, 1917 (2006).
- [25] S. F. King and G. G. Ross, Phys. Lett. B **574**, 239 (2003), I. de Medeiros Varzielas, S. F. King and G. G. Ross, Phys. Lett. B **644**, 153 (2007), Riazuddin, Eur. Phys. J. C **51**, 697 (2007).
- [26] P. Chen, G. J. Ding, F. Gonzalez-Canales and J. W. F. Valle, Phys. Lett. B **753**, 644 (2016).
- [27] P. A. R. Ade *et al.* [Planck Collaboration], Astron. Astrophys. **594**, A13 (2016).

- [28] K.A Olive et al [Particle Data Group] Chinese Physics C38, 090001 (2014).
- [29] G. Ecker, W. Grimus, H. Neufeld, J.Phys. A20, L807 (1987); Int.J.Mod.Phys. A3, 603 (1988). W. Grimus and M. N. Rebelo, Phys. Rept. 281, 239 (1997). G. J. Ding, S. F. King and A. J. Stuart, JHEP **1312**, 006 (2013). C. Hagedorn, A. Meroni and E. Molinaro, Nucl. Phys. B **891**, 499 (2015). P. Chen, C. Y. Yao and G. J. Ding, Phys. Rev. D **92**, no. 7, 073002 (2015).
- [30] R. Samanta, P. Roy and A. Ghosal, Eur. Phys. J. C **76**, no. 12, 662 (2016), R. Samanta, P. Roy and A. Ghosal, Acta Phys. Polon. Supp. **9**, 807 (2016).
- [31] P. Adamson *et al.* [NOvA Collaboration], Phys. Rev. Lett. **118**, no. 15, 151802 (2017).
- [32] P. Chen, G. J. Ding and S. F. King, JHEP **1603**, 206 (2016). R. Samanta, M. Chakraborty, P. Roy and A. Ghosal, JCAP **1703**, no. 03, 025 (2017).
- [33] M. Fukugita and T. Yanagida, Phys. Lett. B **174**, 45 (1986).
- [34] J. M. Cline, [hep-ph/0609145](https://arxiv.org/abs/hep-ph/0609145). W. Buchmuller, P. Di Bari and M. Plumacher, Annals Phys. **315**, 305 (2005), S. Davidson, E. Nardi and Y. Nir, Phys. Rept. **466**, 105 (2008). E. Bertuzzo, P. Di Bari, F. Feruglio and E. Nardi, JHEP **0911**, 036 (2009). V. Barger, D. Dicus, H.-J. He, T. Li, Phys. Lett. B 583 (2004). M.Yu.Khlopov, A.D.Linde, Phys. Lett. (1984), V. 138B. M.Yu.Khlopov, Cosmoparticle physics. World Scientific, 1999.
- [35] G.'t Hooft, Phys. Rev. D **14**, 3442 (1976).
- [36] A. Pilaftsis and T.E.J. Underwood, Nucl. Phys. **B692** (2004) 392. B. Adhikary, M. Chakraborty and A. Ghosal, Phys. Rev. D **93**, 113001 (2016).
- [37] W. Buchmuller, P. Di Bari and M. Plumacher, Nucl. Phys. B **665**, 445 (2003).
- [38] G. Engelhard, Y. Grossman, E. Nardi and Y. Nir, Phys. Rev. Lett. **99**, 081802 (2007).
- [39] A. Abada, S. Davidson, A. Ibarra, F.-X Josse-Michaux, M. Losada and A. Riotto, JHEP **0609** (2006) 010.
- [40] P. Chen, G. J. Ding, F. Gonzalez-Canales and J. W. F. Valle, Phys. Rev. D **94**, no. 3, 033002 (2016).
- [41] C. Hagedorn and E. Molinaro, Nucl. Phys. B **919**, 404 (2017).
- [42] S. Davidson and A. Ibarra, Phys. Lett. B **535**, 25 (2002).
- [43] P. Di Bari and M. Plumacher, Annals Phys. **315**, 305 (2005)
- [44] B. Adhikary, M. Chakraborty and A. Ghosal, JHEP **1310**, 043 (2013) Erratum: [JHEP **1409**, 180 (2014)].

- [45] M. C. Gonzalez-Garcia, M. Maltoni and T. Schwetz, Nucl. Phys. B **908**, 199 (2016)
- [46] W. Rodejohann, Int. J. Mod. Phys. E **20**, 1833 (2011). P. S. Bhupal Dev, S. Goswami, M. Mitra and W. Rodejohann, Phys. Rev. D **88**, 091301 (2013).
- [47] M. Auger *et al.* [EXO-200 Collaboration], Phys. Rev. Lett. **109**, 032505 (2012)
- [48] K. Asakura *et al.* [KamLAND-Zen Collaboration], Nucl. Phys. A **946**, 171 (2016)
- [49] M. Agostini *et al.* [GERDA Collaboration], Phys. Rev. Lett. **111**, no. 12, 122503 (2013)
- [50] B. Majorovits [GERDA Collaboration], AIP Conf. Proc. **1672**, 110003 (2015)
- [51] N. Abgrall *et al.* [Majorana Collaboration], Adv. High Energy Phys. **2014**, 365432 (2014)
- [52] M. Agostini, G. Benato and J. Detwiler, [arXiv:1705.02996](https://arxiv.org/abs/1705.02996) [hep-ex].
- [53] K. Abe *et al.* [T2K Collaboration], Phys. Rev. D **91**, no. 7, 072010 (2015)
- [54] J. Bian [NOvA Collaboration], [arXiv:1510.05708](https://arxiv.org/abs/1510.05708) [hep-ex].